Chapter 1

USE OF GROUND BASED MAGNETOMETERS TO INFER THE
DYNAMICS OF MAGNETOSPHERE-IONOSPHERE COUPLING
AND THE SOLAR-TERRESTRIAL INTERACTION

Gordon Rostoker

Institute of Earth and Planetary Physics and Department of Physics
University of Alberta, Edmonton, Alberta, Canada T6G 2J1

ABSTRACT

For many years, the level of magnetospheric and ionospheric activity has been quantified by the use of ground based measurements of the perturbation magnetic field at selected positions on the Earth's surface. In more recent times, our understanding of how to interpret the magnetic perturbation pattern has allowed researchers to move from the use of crude indices of activity to detailed inferences from arrays of magnetometer data and from individual magnetograms themselves. In this paper, I shall describe how magnetometer data were used in the early days of space research to provide insight into magnetospheric dynamics and solar-wind magnetosphere coupling. I shall then outline modern techniques for conversion of raw magnetometer data into information about ionospheric currents and the field-aligned currents which couple the ionosphere to the distant magnetosphere. I shall also provide schemes by which researchers can use individual magnetograms to infer the position of the auroral oval and the strength of the electric currents flowing along the oval.

INTRODUCTION

At the present time, there are about 100 magnetometers operating continually at observatories distributed irregularly over the Earth's surface. Most of these observatories are sited for reasons other than scientific logic so that one is not dealing with an organized array of instrumentation. Nonetheless, these magnetometers together with some small organized arrays operating in an expeditionary fashion have provided the space research community with an invaluable tool for studying the solar-terrestrial interaction over the past few decades. In the early part of the twentieth century, most research involving ground magnetometer data involved statistical studies of data from single stations. Starting with the pioneering work of Silsbee and Vestine [1942] and Harang [1946], efforts were made to take advantage of accidental arrangements of instruments (eg. magnetometers lying along a line of constant magnetic latitude or longitude) to infer information about localized current distributions in the ionosphere.

The beginning of modern space research is marked by the publication of two foundation stone papers at the start of the 1960's. Around that time, Axford and Hines [1961] and Dungey [1961] presented physically viable pictures of how energy from the solar wind could penetrate the inner magnetosphere and eventually be deposited in the upper atmosphere. The scheme of energy transport within the magnetosphere developed by Axford and Hines was based on the character of the DS equivalent current system, which, in turn, was derived using ground magnetometer data. In fact, countless papers on ionospheric and upper atmosphere research in the early years of space science centered on the estimation of the equivalent current systems for various types of geomagnetic perturbations. One of the first things we shall do in this paper is to describe equivalent current systems and the means by which they are derived.

By the late 1960's some researchers began to set up specific arrays of magnetometers in order to study the dynamic behaviour of the auroral electrojets. Following the research of Bonnevier et al. [1970] using a fortuitous alignment of stations along a line of constant longitude across the average position of the auroral oval, Rostoker et al. and Akasofu et al. set up and operated meridian lines of magnetometers in Canada and Alaska respectively. Some two dimensional arrays were also operated on an expeditionary basis during the 1970's which were used for the study of upper atmospheric current systems (e.g. Bannister and Gough, 1977). While meridian lines of magnetometers were useful in delineating the latitudinal structure of the auroral electrojets, it was ultimately necessary to establish east-west aligned magnetometer lines to study the azimuthal structure in the electrojets and in the associated auroral luminosity. Such arrays were constructed by Rostoker et al. and by Baumjohann et al. in Canada and Scandinavia respectively and have been particularly useful in the study of ULF magnetic pulsations and substorm expansive phase activity. In the second part of this paper, I shall outline the data presentation modes for meridian line and east-west line data and suggest inferences which can be made from such data sets regarding ionospheric and field-aligned currents.

During the 1980's, large computers began to play an increasingly important role in the process whereby researchers convert knowledge of ground based magnetometer data into information about the real currents flowing in the magnetosphere-ionosphere system. Taking advantage of this evolving computational tool, Richmond et al. in the U.S.A. and Mishin et al. in the U.S.S.R. began to develop algorithms for evaluating the instantaneous real current distributions using as input data the ground magnetometer data and a model ionospheric conductivity distribution. In the final part of this paper, I shall outline the technique for such current system estimations following the approach of Kamide et al. [1981], which is known as the KRM method.

MEASUREMENTS OF THE PERTURBATION MAGNETIC FIELD AT THE EARTH'S SURFACE

It would be ideal if all magnetometers recording at the Earth's surface used the same coordinate system in which to represent their data. Unfortunately, such is not the case with the data being recorded in two primary coordinate systems and subsequently being portrayed in the literature in several other coordinate systems after appropriate coordinate transformations. The two primary systems for the recording of data are:

(1) Geographic where the X component is defined as positive northward, the Y component is defined as positive eastward and the Z component is defined as positive downward.

(2) Local magnetic where the H component is defined as positive northward, the D component is defined as positive eastward and the Z component is defined as positive downwards.

While the X component lies in the geographic meridional plane, the H component lies in the local magnetic meridian plane. Figure 1 shows the geometrical arrangement of the relevant coordinate axes for the geographic and local magnetic coordinate directions. In addition, it should be noted that researchers often portray their perturbation vectors in the centered dipole coordinate system $(X_m, Y_m, and Z)$ where X_m is positive pointing toward geomagnetic north, Y_m is positive towards geomagnetic east and Z is positive

downwards. The horizontal axis directions are also shown in Figure 1 and the coordinate transformation equations from local magnetic to geographic and local magnetic to centered dipole are respectively

$$\Delta X = \Delta H \cos D - (H_o \Delta D) \sin D$$
$$\Delta Y = \Delta H \sin D - (H_o \Delta D) \cos D \qquad (1)$$

$$\Delta X_m = \Delta H \cos (D - \Psi) - H_o \Delta D \sin (D-\Psi)$$
$$\Delta Y_m = \Delta H \sin (D - \Psi) + H_o \Delta D \cos (D-\Psi) \qquad (2)$$

where H_o is the total horizontal field strength, D is the magnetic declination measured in degrees and Ψ is the great circle distance from the geomagnetic to the geographic pole measured in degrees. Other more elegant coordinate systems such as corrected geomagnetic coordinates (taking into account the quadrupole components of the main field) are also used from time to time (viz. Hakura, 1965); however these are more difficult to deal with since the systems may not be orthogonal. The centered dipole system appears to be the most effective orthogonal coordinate system in which to order ground magnetometer data to this point in time.

In general, one categorizes magnetometer locations as either high latitude, auroral zone or low latitude. Implicit in these categorizations is the assumption that:

(1)   High latitude means that the observing station is poleward of the high latitude edge of the auroral oval. (One cannot assign a specific lower latitude to the "high latitude" region, because the auroral oval grows and shrinks with changing levels of magnetospheric activity.)

(2)   Auroral zone means that the observing station lies inside the auroral oval (i.e., ionospheric electrojet current flows over the observing station).

(3)   Low latitude pertains to the region extending from the equatorward border of the auroral oval to the Earth's magnetic equator.

Although the term "middle latitude" also is found in the literature, there is no physical basis for breaking up the region between the equatorward edge of the auroral oval and the geomagnetic equator into two distinctive regions. There is some reason to believe that some interesting physical processes take place at the plasmapause (which lies equatorward of the auroral oval); however the term "middle latitude" does not apply to a region one of whose boundaries is the plasmapause.

Figure 2 shows typical magnetograms from stations located in the three regions described above. In this case, the perturbations are measured in the geographic coordinate system but in central Canada (where the observatories are located), the local magnetic north and geographic north directions are almost the same. These data were taken digitally and have been subsequently put into the analogue form shown here. However, there still are many stations in the global network which record on strip chart. The different recording techniques used at the various observatories around the world makes quantitative analysis of the magnetic perturbation data more difficult than one would like. Inspection of Figure 2 reveals that the magnetic perturbation pattern for the same
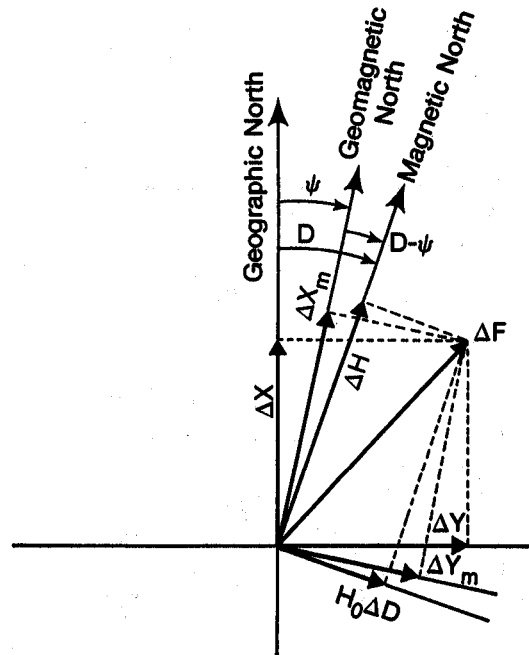
Figure 1. Relationships among the various coordinate systems used to display ground based geomagnetic data. The coordinate transformations between systems are shown in Eq. (1).
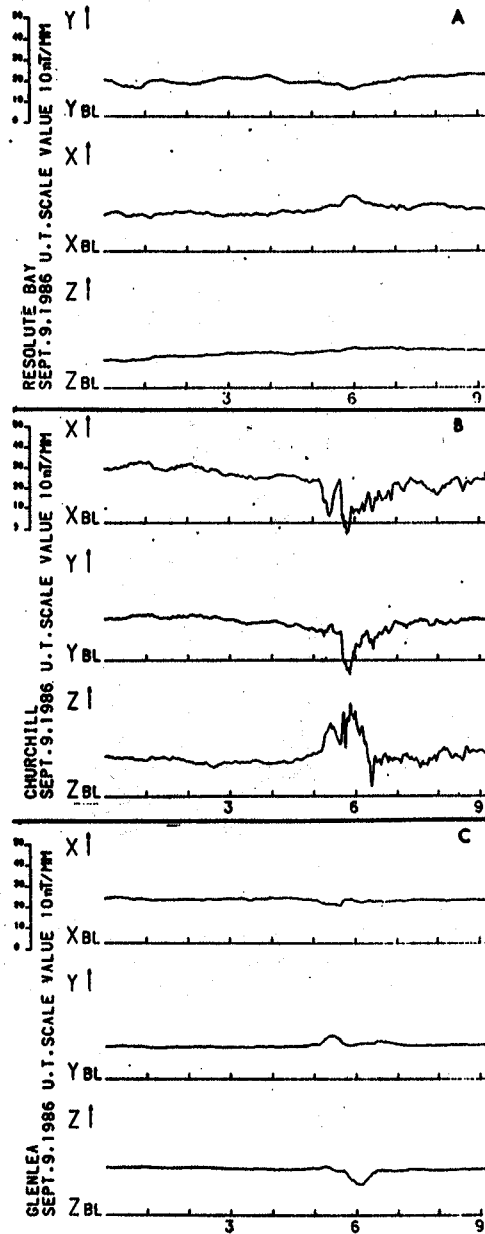
Figure 2. Three typical magnetograms displaying a substorm event as viewed at high latitude (A), auroral oval (B) and subauroral (C) stations. Magnetospheric substorm disturbances are seen between 0500 and 0700 UT. Stations well outside the oval see predominantly the effects of field-aligned currents.

period of time is quite different in the three different zones alluded to above. This demonstrates unambiguously that the electric current systems being monitored can be spatially quite localized.

One can immediately appreciate that a full description of an individual event would require the presentation of an unreasonable amount of magnetometer data if these data had to be expressed in the form shown in Figure 2. For this reason, researchers developed methods of portraying the essential information in a more compact form. The first of these modes of presentation to gain favour was the equivalent current system. Figure 3 shows a typical equivalent current system for relatively disturbed times. In the construction of such a figure, it is assumed that the magnetic perturbations everywhere are due solely to ionospheric currents. The strength of the current over each site is estimated by assuming that the horizontal magnetic perturbation vector is due to an infinite sheet overhead current with often no correction for Earth induction being considered. The current vectors shown on the figure have a magnitude proportional to the inferred current density and the current vectors are oriented normal to the magnetic perturbation vectors. The equivalent current contours are sketched in a fashion so that the strength of the equivalent current is inversely proportional to the distance between the current lines. This mode of presentation is compact, however it contains no information regarding the vertical component of the perturbation magnetic field. As we shall see, the Z-component of the perturbation magnetic field can be extremely useful in inferring the properties of the real currents flowing in the magnetosphere-ionosphere system.

Another way in which magnetospheric activity levels have been quantified using magnetometer data is through the development of geomagnetic indices. The primary ones used in the past are the K_p, Dst and AE indices. (The reader is referred to Rostoker [1972] for a detailed description of the derivation of these indices.) At the present time, only the AE index is used extensively so that I shall only summarize the origins of that index. The process of creating the index involves the use of the magnetograms from 12 stations distributed in a relatively uniform fashion around the world at average auroral zone latitudes. The traces of the north-south component are superposed on one another and at each minute, the maximum positive value and the maximum negative value of the 12 traces are chosen. The time series of maximum positive values is called AU while the time series of maximum negative values is called AL. The sum of the absolute values of AU and AL at each minute has been termed AE. A sample daily record of the AU, AL and AE indices is shown in Figure 4. It is important to realize that the time series of the AU, AL and AE indices have no physical meaning as they do not reflect the intensity variation of any particular magnetosphere-ionosphere current system. The AU index is a crude estimator of the lower limit of the strength of eastward flowing ionospheric current (which creates a positive deflection in the north-south component of the perturbation magnetic field below the ionosphere) while the AL index reflects the strength of the westward flowing ionospheric current (creating a negative deflection in the north-south component of the perturbation magnetic field). The AE index crudely quantifies activity level but yields no information about what current systems may cause that activity.

There are several weaknesses in the formulation of the AU, AL and AE indices which makes their use risky in any way other than establishing a lower limit to the magnetospheric activity level. The problems are:
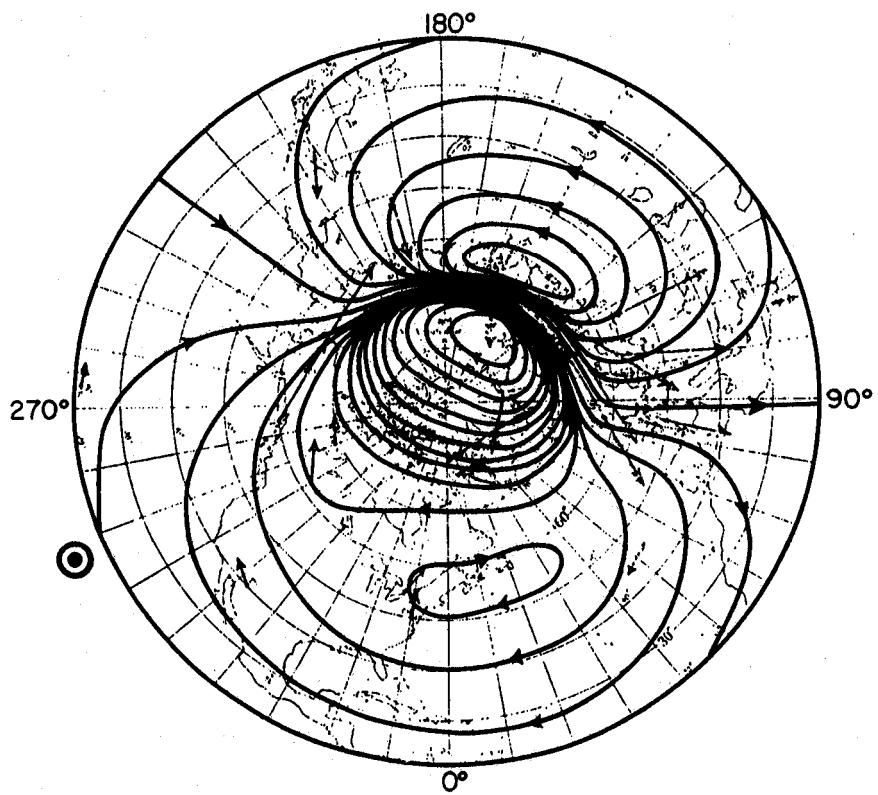
Figure 3. Equivalent current system for a polar magnetic sub-
storm (Fukushima, 1953). The distance between current lines
is approximately inversely proportional to the strength of the
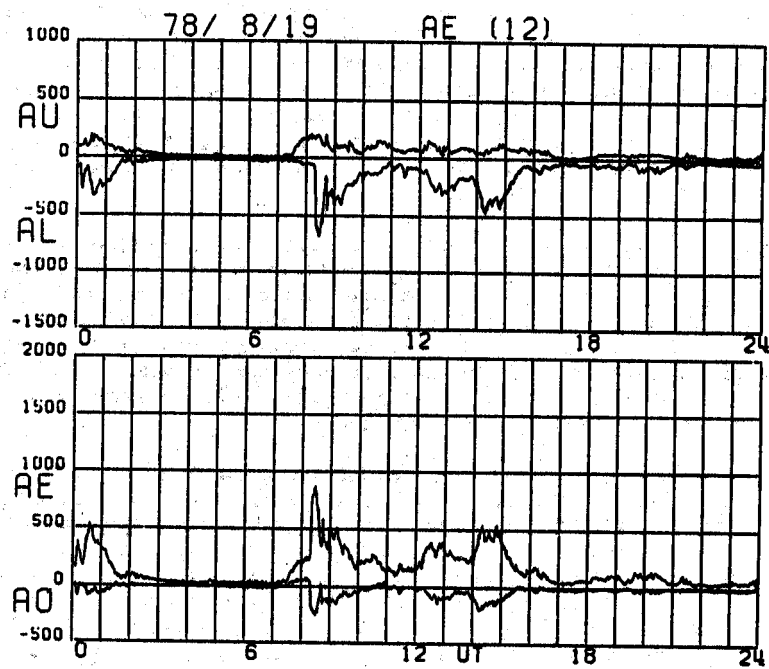equivalent overhead current.

Figure 4. Typical records of AE, AU and AL over the period of one day during which magnetospheric substorm activity was in evidence.

1. There is a high probability that no AE station is located at the locale of
    the true maximum magnetic perturbation at the earth's surface. This is
    because, during quiet times, the contracted auroral oval typically lies
    poleward of the AE stations while, during active time the currents flowing
    in the oval may lie equatorward of the AE stations. Figure 5 shows values
    of the AE index for one day where the normal AE (created from the data of
    12 stations) could be compared with an AE index created using a network of
    70 stations. It is evident that the magnetic activity level can often be
    much larger than the normal AE values might suggest (which is particularly
    evident from the two AE traces in the Universal Time interval 1700 –
    2300 on March 18, 1978).

2. It is usual for the researcher to associate the geomagnetic activity index
    with the strength of convection (and hence the strength of the convection
    electric field) in the magnetosphere. However, the magnetic perturbations
    reflect the convolving of electric field and conductivity at each point in
    the ionosphere. During significant enhancements of the magnetosphere-
    ionosphere interaction, the conductivity can become markedly enhanced in
    the midnight sector so that large ionospheric currents can be produced
    with relatively weak electric fields.

3. The magnetic perturbations of field-aligned currents are superposed on the
    magnetic fields produced by the ionospheric currents, tending to reduce
    the estimate of the overhead current being remotely sensed by the AE
    stations. Figure 6 shows a cartoon of a three-dimensional current system
    believed to flow during major auroral outbursts in the midnight sector.
    It is clear that the magnitude of the north-south component of the pertur-
    bation magnetic field due to the ionospheric current is reduced due to
    contributions from the field-aligned currents linking the ionospheric
    currents to the outer magnetosphere.

4. There is no way in which the changes in magnetic field due to the spatial
    motion of localized current systems can be separated from changes in the
    actual magnitudes of the current flow in those systems. For example, a
    decrease in the AU index may simply reflect the equatorward motion of a
    latitudinally localized eastward current from directly overhead to some
    position well distant from the AE station.

For these reasons, any researcher wishing to study the details of some indiv-
idual event in terms of establishing the nature of the magnetosphere-ionosphere
current system ought not to use the indices but rather should study the
individual magnetograms from relevant stations.

THE ELECTRIC CURRENT SIGNATURES OF THE COMPONENTS OF MAGNETOSPHERIC SUBSTORM
ACTIVITY

    The electric current systems which couple the distant magnetosphere to the
ionosphere play a vital role in regulating the energy flow within the magneto-
sphere and the ultimate degradation of high grade bulk flow energy into low
grade heat. It is generally believed that solar wind plasma makes its way from
the magnetosheath into the boundary layers just inside the magnetopause (cf.
Eastman et al., 1985). Within the boundary layers, the convective bulk flow
energy of the plasma is extracted through magnetohydrodynamic (MHD) generator
processes (cf. Lundin, 1988) and converted to the electromagnetic energy of the
three-dimensional current systems which couple the ionosphere and magneto-
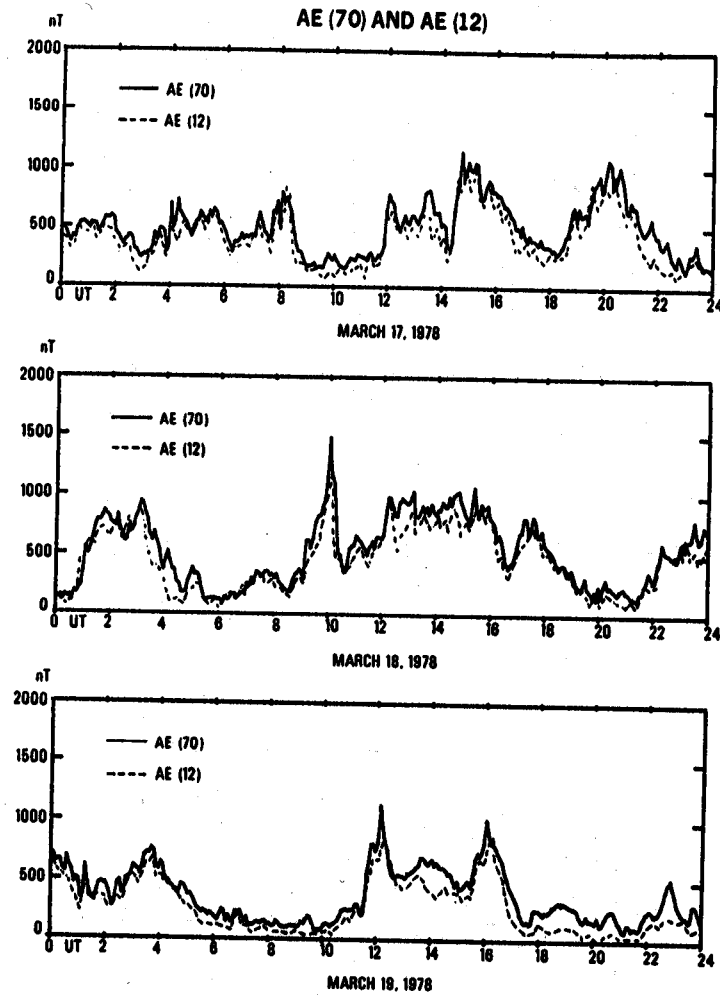sphere. Ultimately, this electromagnetic energy is converted to heat through

Figure 5. Comparison of AE computed using data from the 12 normal stations with AE computed using data from 70 ground observatories distributed over the Earth's surface (Kamide et al., 1982). The 12 station index clearly underestimates the activity level, particularly in the interval after 1800 UT on March 19, 1978.
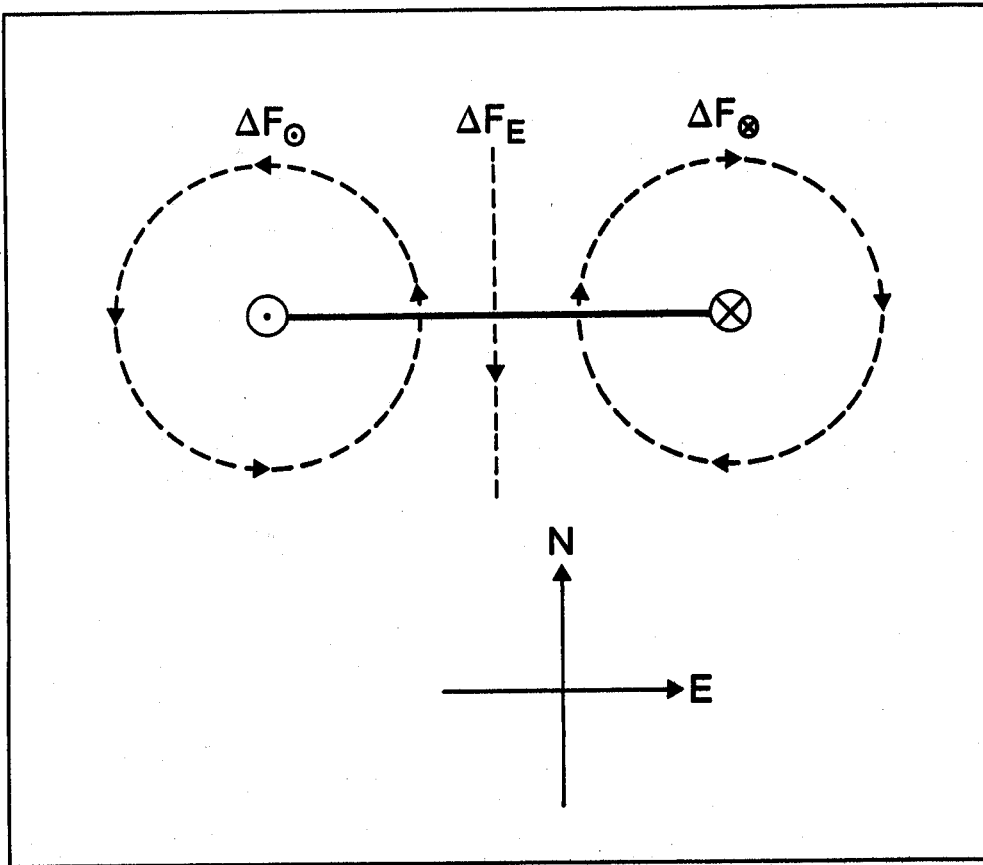
Figure 6. Equivalent three dimensional current system assoc-
iated with the substorm current wedge observed during
expansive phase activity. The magnetic perturbations from the
field-aligned and ionospheric currents clearly oppose one
another directly under the ionospheric electrojet.

Joule heating associated with Pedersen current flow in the auroral ionosphere. The concurrent heating of plasma in the central plasma sheet through both adiabatic processes (Hines, 1963) and non-adiabatic processes (Goertz and Smith, 1989) leads to pressure gradients. Once again, MHD generator processes lead to both inertial and diamagnetic currents being driven in the central plasma sheet and these can be connected to the auroral ionosphere by Birkeland currents thus allowing energy to be extracted from the magnetospheric plasma (cf. Rostoker and Boström, 1976). In this fashion, the plasma sheet is cooled and the upper atmosphere is heated.

The electric current systems described above fluctuate in response to changes in the interplanetary medium. Perrault and Akasofu [1978] have defined the epsilon parameter which gives a reasonable quantitative measure of the amount of energy which penetrates the magnetosphere in terms of the relevant interplanetary parameters, viz.

$$\epsilon = \ell_0^2 \, v \, B^2 \sin^4 \frac{\Theta}{2} \tag{3}$$

where v is the solar wind speed, B is the magnitude of the interplanetary magnetic field, Θ is the polar angle of the component of the IMF normal to the sun-earth line and measured from the northward geomagnetic axis and $\ell_0 (\sim 7R_E)$ is a constant with the dimensions of distance. While v and B normally do not change by factors of more than two, the angle Θ can change by as much as $180°$ in a matter of seconds and often does so. Thus the amount of energy entering the magnetosphere is strongly modulated by the direction of the IMF with maximum entrance of energy occurring for $\Theta = 180°$ (purely southward IMF) and minimum entrance of energy occurring for $\Theta = 0°$ (purely northward IMF). It is common to study episodes of enhanced magnetospheric activity, such as those seen in Figure 4. Such episodes have been labeled magnetospheric substorms and the study of substorm magnetic signatures is still a very active research area. For this reason it is useful to spend some time is describing the various aspects of substorm activity.

Figure 7 shows the evolution of auroral activity as the auroral oval experiences an episode of magnetospheric substorm activity. The large scale behaviour of the oval involves an equatorward expansion during the period when the IMF has become more southward and a contraction to its previous location when the IMF returns to its previous orientation. (This is equivalent to ϵ increasing and subsequently decreasing back to its original value.) During the period of enhanced energy input from the solar wind, the oval can brighten and distorted discrete auroral forms called surges can appear from time to time on its poleward border in the evening sector. At the same time, electric current strength increases along the high conductivity channel marked by the auroral luminosity which defines the oval. The ionospheric current flow is eastward across the dusk meridian and westward across the dawn meridian. These two ionospheric currents along with their associated closure currents in the magnetosphere constitute the directly driven component of substorm activity. At the same time as the directly driven system of currents grows, energy is also stored in the magnetotail with this storage feature of the substorm being called the growth phase. The return of ϵ to its pre-substorm value can often lead to explosive discrete auroral arc development in the midnight and evening sector of the oval. This often violent auroral activity is accompanied by a poleward motion of the poleward edge of the oval. The beginning of this poleward motion marks the onset of the substorm expansive phase. The expansive phase features many individual arc formations of limited longitudinal extent
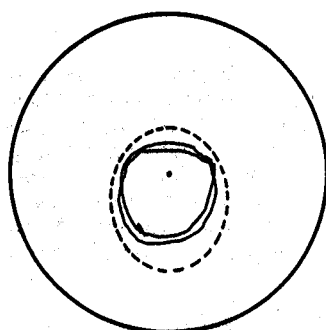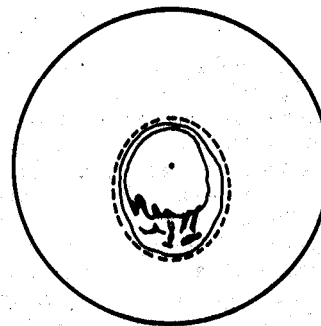
IMF after being northward
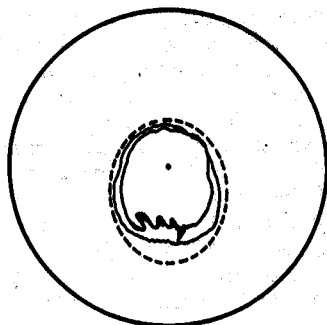for some time has just
turned southward
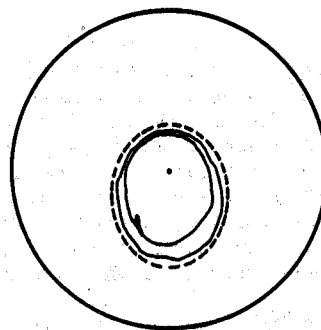
Oval expands equatorward
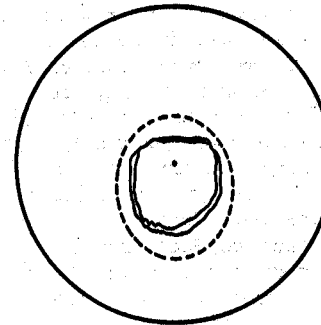under influence of
southward IMF
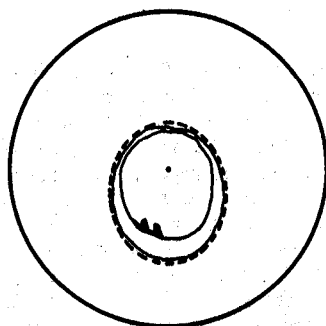
IMF has just turned
northward

Poleward edge of oval
expands poleward and
features multiple surges.
Bright structures seen
within diffuse evening auroras

Surge action at poleward
edge of oval continues as
diffuse auroras recede poleward

Return to quiet oval about 1
hr after IMF northward turning

Figure 7. Sequence of plots of the auroral oval during the
growth and recovery of a magnetospheric substorm. Auroral
surges are found at the poleward edge of the oval, with the
size of the polar cap being regulated by the Bz component of
the interplanetary magnetic field (Rostoker, 1989).

and featuring a surgelike structure at their western edges. Each of these surges is the site of field-aligned current flowing out of the ionosphere. This field-aligned current is fed predominantly by a westward electrojet coming from regions to the east of the surge form. The combination of the magnetic effects of the upward field-aligned current and the ionospheric currents in its immediate vicinity produces a unique magnetic signature which we shall discuss later in this paper. The immediate cause of the distorted discrete auroral features is thought to be the release of energy from the magnetotail which was stored during the growth phase. The combined storage-release process constitutes the loading-unloading component of substorm activity.

MAGNETIC PERTURBATION PATTERNS OF MAGNETOSPHERE-IONOSPHERE CURRENT SYSTEMS

Before looking at the details of the magnetic signatures of directly driven activity and the unloading of magnetotail energy, it is useful to look at the magnetic perturbations due to some simple current configurations involving ionospheric current flow. Figure 8a shows a latitude profile of an infinite line current flowing westward in the ionosphere at a latitude of 70° N. One finds a negative H-component perturbation directly under the current system which falls off to zero toward lower and higher latitudes. The Z-component reverses polarity across the latitude where the line current flows, with a positive perturbation to the north and a negative perturbation to the south. Had the line current been directed eastward in the ionosphere, the polarities of all the perturbations shown in Figure 8a would have been reversed. Note that, because the line current is of infinite length, there is no D-component perturbation for this system. Figure 8b shows the magnetic perturbation pattern that would have been expected had the ionospheric current flowed from south-west to north-east rather than being purely westward. Now one can see perturbations in both the H-component and D-component, however the peak is located at the same latitude for both components.

We now consider the magnetic perturbations from a three-dimensional current system such as that shown in Figure 9. Profiles for a number of representative meridians are shown in Figure 10 as calculated using the algorithms developed by Kisabeth and Rostoker [1977]. One can immediately see that the extremum values in the Z-component perturbation mark the borders of the westward current flow (which is of finite latitudinal extent) while the polarities of the D-component give information as to whether the observing stations are poleward or equatorward of the center of the westward electrojet and to the east or west of the meridian which bisects the electrojet (which is of finite latitudinal extent). It is also noticeable that the extremum values in the D-component lie just equatorward and poleward of the borders of the ionospheric electrojets, with the magnitude of the perturbation falling off slowly as one moves to lower and higher latitudes respectively. At middle latitudes, the D-component is clearly dominant, the H-component has reversed polarity (as the field-aligned current begins to dominate the ionospheric electrojet current) and one can barely see the edge effect of the electrojet in the weak Z-component perturbation.

MAGNETIC SIGNATURES OF THE DIRECTLY DRIVEN SYSTEM

As we pointed out in the previous section, the directly driven system features an eastward electrojet flowing across the dusk meridian and a westward electrojet flowing across the dawn meridian. The electrojets produce perturbations in the horizontal component of the magnetic field ranging from tens of nT during quiet times to a thousand nT or more during active periods.
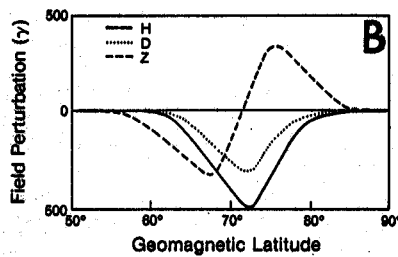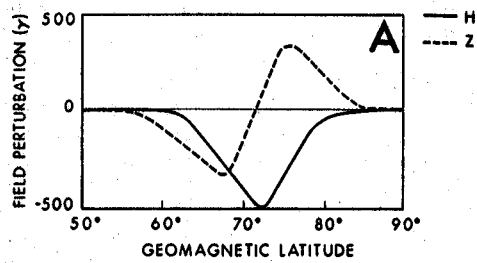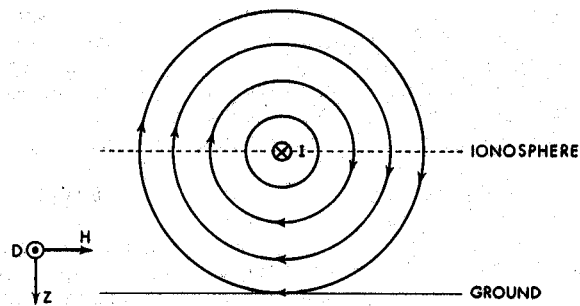
Figure 8. Panel A shows a cartoon of the latitude profile of magnetic disturbance due to an infinite westward ionospheric line current flowing normal to the line of recording magneto-meters (Rostoker, 1972b). Panel B shows a similar profile where the current flows at an angle to the normal to the magnetometer line.
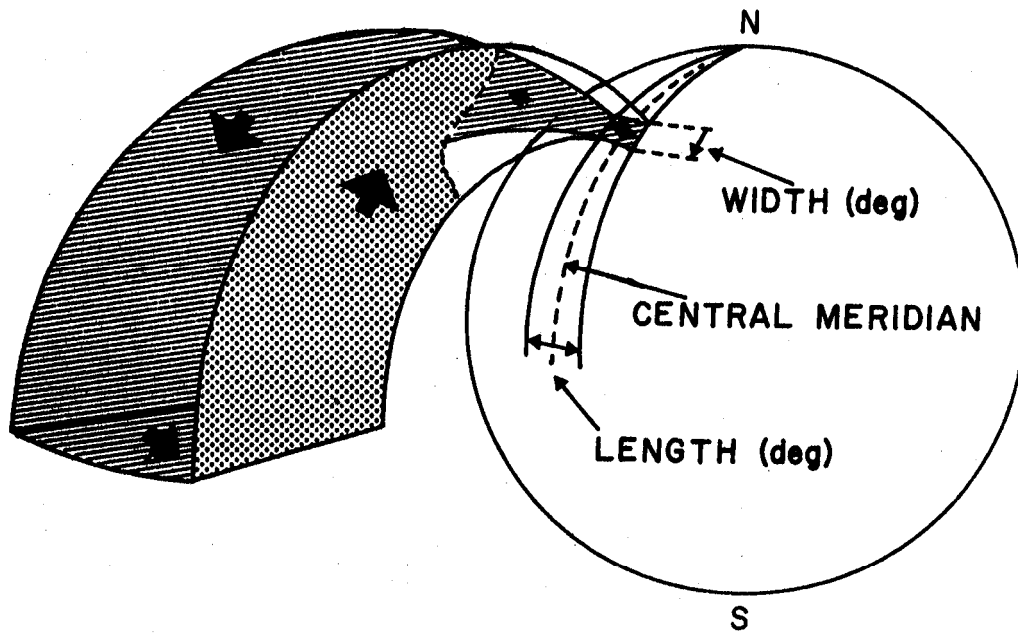
Figure 9. Three-dimensional current system in dipole field geometry representative of the expected current flow associated with substorm expansive phase activity (Kisabeth and Rostoker, 1977).
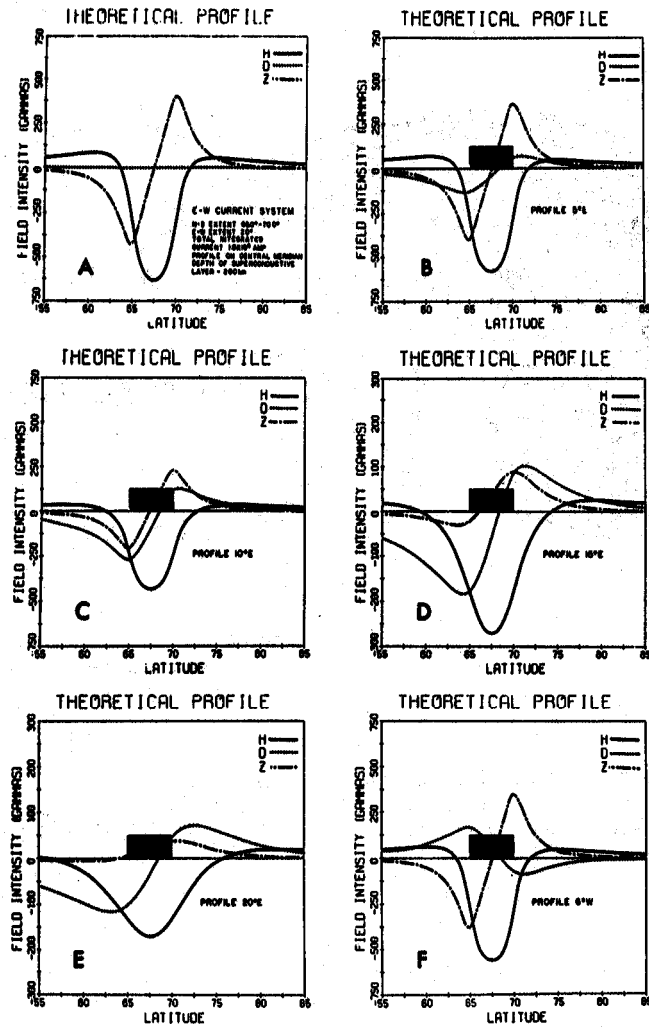
Figure 10. Latitude profiles showing magnetic perturbation patterns along various meridians east and west of the central meridian of the substorm westward electrojet (Kisabeth, 1972). These profiles include contributions due to induced currents in the Earth as described in the text.

Figure 11 shows the expected magnetic perturbation pattern along meridians in several representative magnetic local time sectors. These profiles were prepared by Hughes and Rostoker [1979] using meridian line data taken over several months in the northern hemisphere winter. Their preparation involved the identification of the center of the electrojet (viz. the latitude where $\Delta Z = 0$) and performing the equivalent of a superposed epoch analyses using the center of the electrojet as the key location.

It is evident that the directly driven system involves a clear eastward electrojet across the dusk meridian and a westward electrojet across the dawn meridian as evidenced from the H-component and Z-component profiles (see Figure 8). The typical widths of those driven system electrojets is ~6° of latitude (viz. ~600-700 km) during average levels of activity. Near noon it is difficult to detect clear electrojet signatures while in the evening sector near midnight, one finds the signature of a westward electrojet current lying at the poleward edge of an eastward electrojet. (It is worth noting that the evening sector westward electrojet can experience large rapid transient changes in both width and magnitude. Then changes are associated with substorm expansive phase effects which will be discussed later in this paper.) While the H- and Z-components of the magnetic perturbation patterns shown in Figure 11 give vital information about overhead electrojet currents, the D-component gives much information about field-aligned currents penetrating the auroral oval and any azimuthal asymmetries in ionospheric current flow. In particular, the level shift in the D-component going from north to south in the noon sector indicates net downward field-aligned current flow across the local time regions, while the level shift in the D-component across the late evening sector indicates net upward field-aligned current. Current densities of these field-aligned currents have been established empirically by Hughes and Rostoker [1979] and can be evaluated for individual events through assumption of a reasonable forward model for the global current system involved in magneto-sphere-ionosphere coupling (cf. Rostoker and Mareschal, 1981).

Finally, it should be noted that the net field-aligned current sheets described above create a distinctive magnetic signature over the polar cap region. In the early days of magnetospheric research, this magnetic signature was attributed to overhead electric current flow in the polar cap ionosphere. Ultimately, Heppner et al. [1971] were able to demonstrate that the polar cap magnetic signature was primarily due to the field-aligned current sheets which reflect the net upward and downward current flow across the evening and noon sectors respectively. This is an excellent example of a situation where equivalent current flow (across the polar cap) does not reflect the actual overhead flow of real electric current.

MAGNETIC SIGNATURES OF SUBSTORM EXPANSIVE PHASE ACTIVITY

The base substorm expansive phase current system is often called the "substorm current wedge" and is viewed as an ionospheric westward electrojet across the midnight region linked to the magnetosphere by current into the ionosphere at its eastern edge and out of the ionosphere at its western edge (cf. Figure 12). The magnetic signatures of this current loop as seen in the three components of the perturbation magnetic field are shown in magnetogram format in Figure 13 for various locations of observations on the nightside of the earth. In the context of this cartoon, the evolution of the current wedge involves spreading of the ionospheric electrojet both eastward and westward, although the westward spreading is viewed as dominant. Thus, the central meridian (bisecting the ionospheric electrojet) is found to move westward as
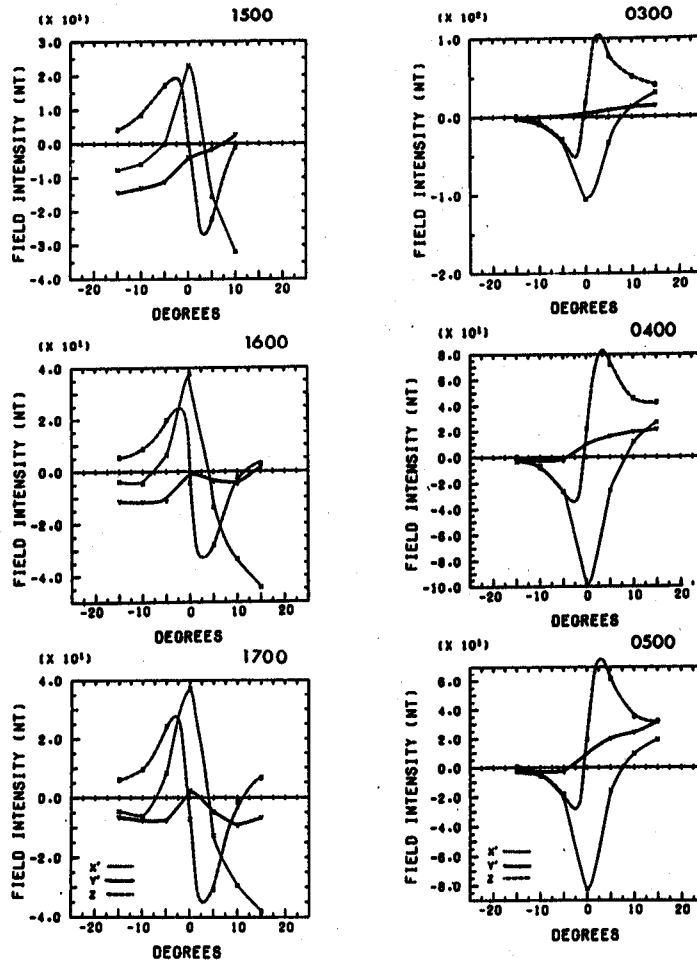
Figure 11. Averaged profiles in various magnetic local time
sectors computed from three months of hourly averaged values
from a meridian line of stations keyed to the center of the
electrojet crossing the meridian. The panels on the left hand
side of the figure are representative of afternoon sector pro-
files (MLT given at the top of each panel) while those on the
right side of the figure are for the morning hours (Hughes and
Rostoker, 1979).
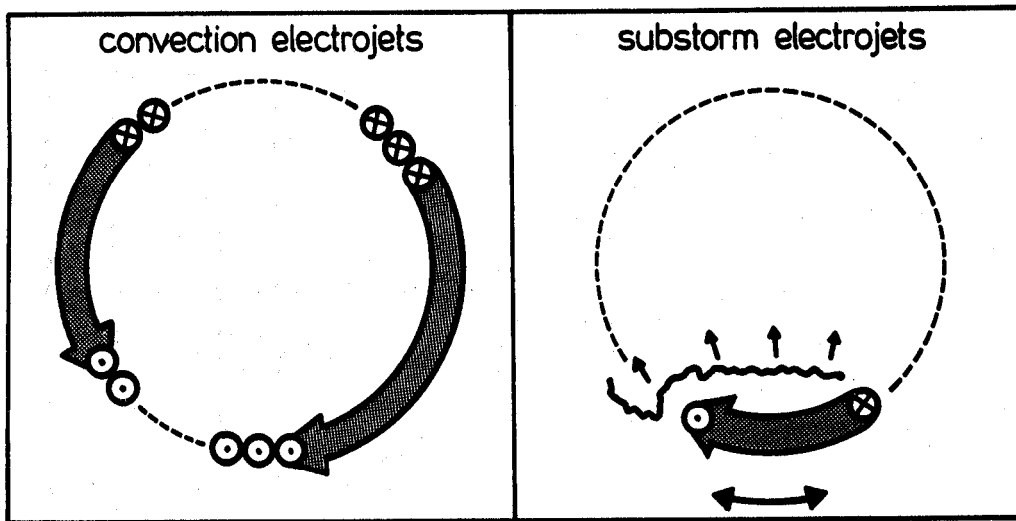
Figure 12. Cartoon representation of the substorm current wedge placed in the context of the directly driven auroral electrojets (Baumjohann, 1983).

LOCATION OF OBSERVATORY	ONSET TO EAST OF OBSERVATORY	ONSET ON MERIDIAN OF OBSERVATORY	ONSET TO WEST OF OBSERVATORY
NORTH OF CENTER OF WESTWARD ELECTROJET	HA DA ZA		
SOUTH OF CENTER OF WESTWARD ELECTROJET	HA DA ZA		
LOW LATITUDES	HA DA		
	O A R	O&A R	O R
CODE	O - ONSET OF SUBSTORM A - ARRIVAL OF SURGE AT OBSERVATORY MERIDIAN R - ONSET OF RECOVERY		

Figure 13. Magnetic signatures of the development of the substorm current wedge at various locations on all sides of the current configuration. The placement of the auroral oval observatory closest to the local time of expansive phase onset is such that the initial surge formation is slightly to the east of the observation point (Rostoker et al., 1980).

the substorm expansive phase evolves (Rostoker et al., 1979) leading to transition D-component bays at subauroral latitudes (Rostoker, 1966) where the D-component d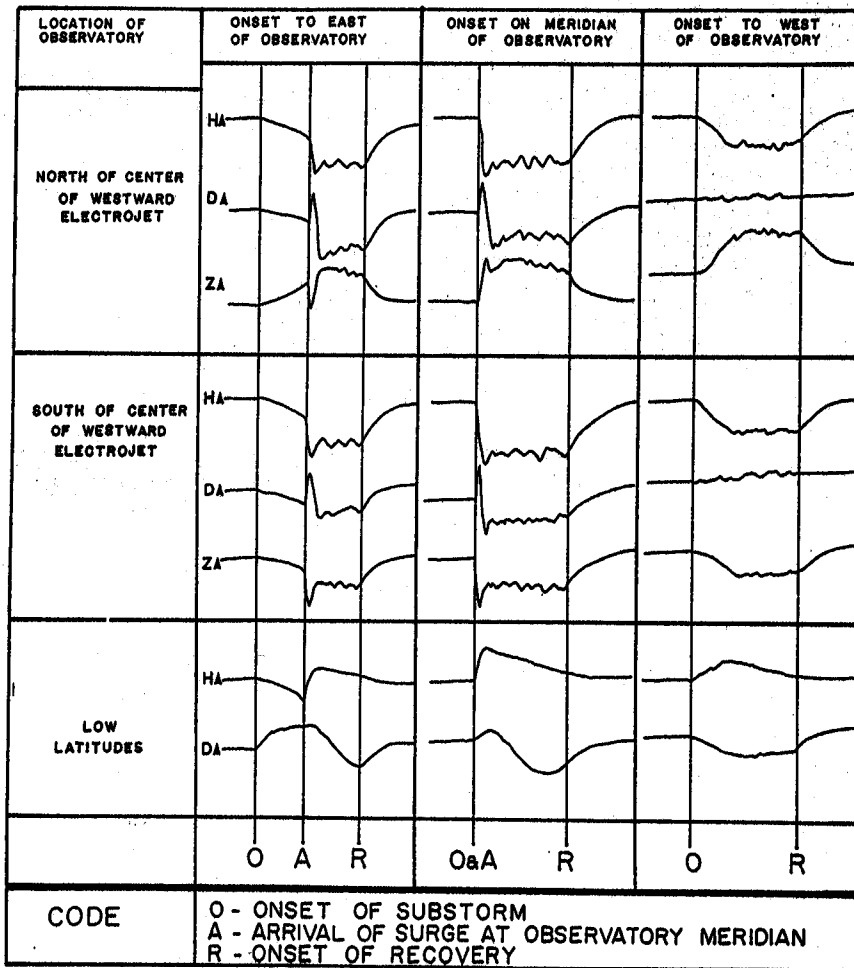eflects first positively and then negatively at an appropriately placed station sometime during the lifetime of the expansive phase.

While the picture of a monolithic wedge suffices for the interpretation of subauroral magnetograms, it is quite inadequate in permitting interpretation of ground magnetic data in the substorm-disturbed region of the auroral oval. This is because the overall substorm expansive phase current system evolves through the appearance of many small scale filamentary current systems whose combined magnetic perturbations yield the impression of a large scale current wedge when detected some distance from the disturbed region. Figure 14 shows, schematically, a typical distribution of these localized current loops after several minutes of expansive phase evolution. Each current element forms, normally, poleward of the previous one and with its western edge further to the west of the previous one. The western edge of each current filament often features a distorted auroral form called a surge. Figure 15 shows the latitude profiles during the evolution of a large substorm expansive phase. These profiles clearly show the poleward expansion of the substorm disturbed region and the multiple peaks in the H-component are clear evidence of the multi-filament character of the evolving substorm westward electrojet.

Fig. 16 shows a magnetogram which features a single isolated substorm filament. This magnetogram yields some information on the lifetime of an individual filament (i.e. several minutes) and the magnitude of its associated magnetic perturbation (~150-200 nT in the H-component directly under the filament). The physics of the substorm expansive phase comes from the study of the development of the individual filamentary current systems rather than the large scale wedge structure (which reflects the overall magnetic perturbation pattern due to the several contributing, filamentary systems). The magnetic signature of an individual filament greatly resembles that of the larger scale current wedge, however for a single filament the magnetic perturbation is barely detectable further than a few degrees from the ionospheric current channel. (Subauroral stations detect substorm expansive phases only when several filaments co-exist, so that their magnetic effects are additive.) Close to a filament the overall magnetic perturbation is dominated by iono-spheric current flow, viz. a latitudinally and longitudinally localized west-ward electrojet producing a negative H-component bay. Near the western edge of the filament, a circulating Hall current around the localized region of upward current flow produces the characteristic signature of a positive D-component perturbation at the western edge of the associated auroral surge and a negative D-component to the east of the center of the upward field-aligned current (Tighe and Rostoker, 1981). Positive D-component bays can, however, result from either growth of the upward field-aligned current (detectable up to hundreds of km from the region of ionospheric outflow) or from the equatorward ionospheric current flow at the western edge of the surge (normally dominating a region of a scale size of ~200 km or less). An absence of significant Z-component fluctuations generally indicates that a positive D-component bay is attributable to the distant effect of field-aligned currents rather than nearby equatorward ionospheric current flow.

Finally, it is useful to comment on the impulsive magnetic pulsations known as Pi 2's. Following the early study of Saito [1961], Pi 2's (or pt's as they were known at that time) were considered to accompany geomagnetic bays observed at subauroral latitudes on a one-to-one basis. Subsequently, Rostoker [1968] demonstrated that a bay-type disturbance might feature several Pi 2
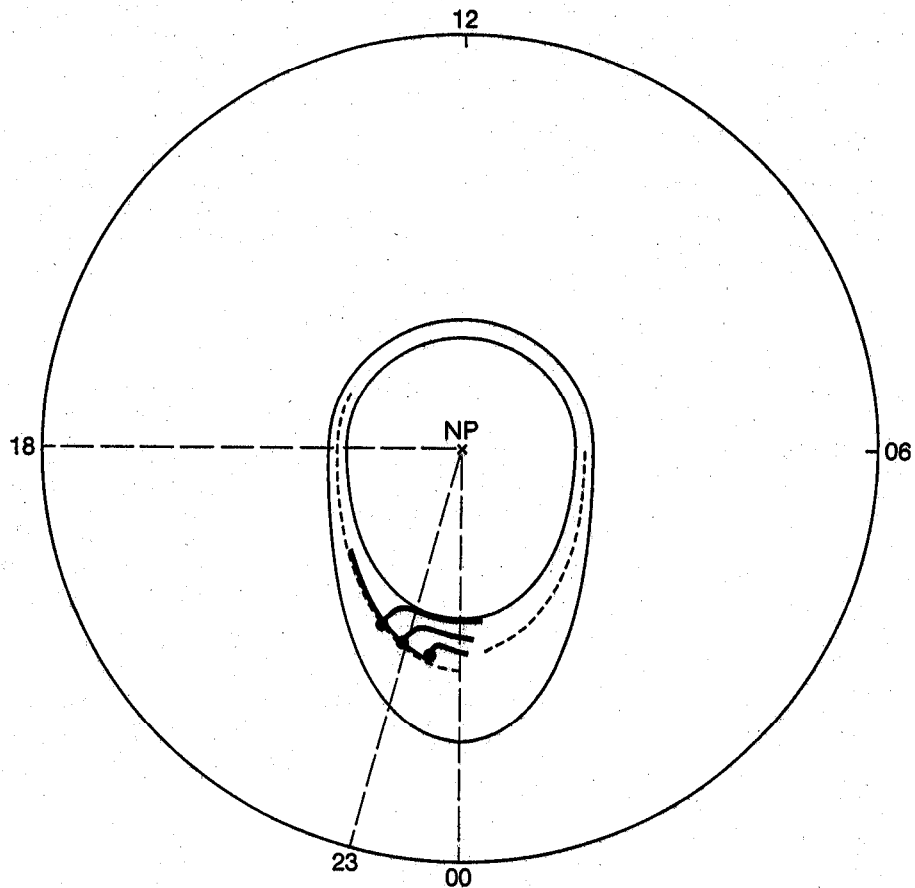
Figure 14. Cartoon showing the development of the filamentary
current elements, the ensemble of which produce the magnetic
signature of the substorm current wedge. Appropriately placed
observatories yield magnetic signatures which clearly show the
wedge to be composed of these small scale structures which
tend to appear near midnight at expansive phase onset and are
seen progressively westward and poleward as the expansive
phase develops. The western edge of each structure is the
site of upward field-aligned current while downward field-
aligned current is distributed diffusely along the track of
the westward electrojet element to the east.
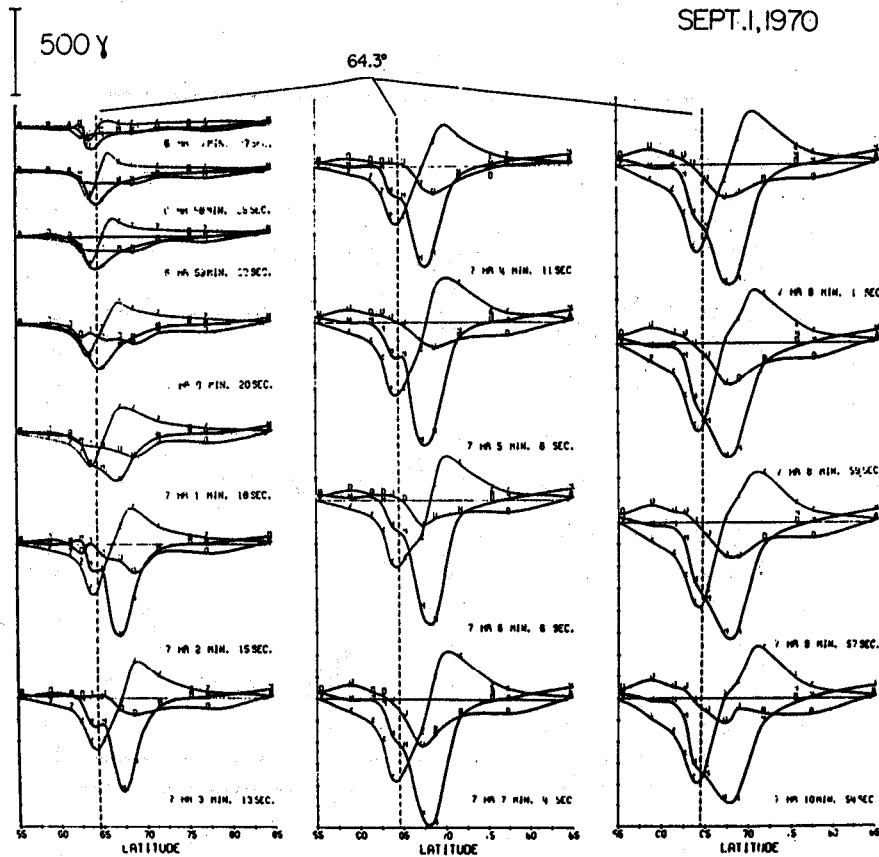
Figure 15. The sequential development of a substorm expansive phase as depicted by a series of latitude profiles taken throughout the episode of poleward expansion (Kisabeth and Rostoker, 1974). The complex structure of the H- and Z-components clearly show the electrojet to typically be a group of narrow channels of westward flowing current rather than a featureless westward sheet current.

Figure 16.   Magnetogram from an auroral oval observatory
featuring the onset and evolution of a single filamentary
structure at approximately 0117 UT on April 3, 1986.   Many of
these filaments occurring in close succession produce the
overall signature of the substorm current wedge.

pulsation bursts, leading eventually to the concept of multiple onset substorms (cf. Wiens and Rostoker, 1975; Pytte et al., 1976). In recent times, it has become apparent that each expansive phase onset or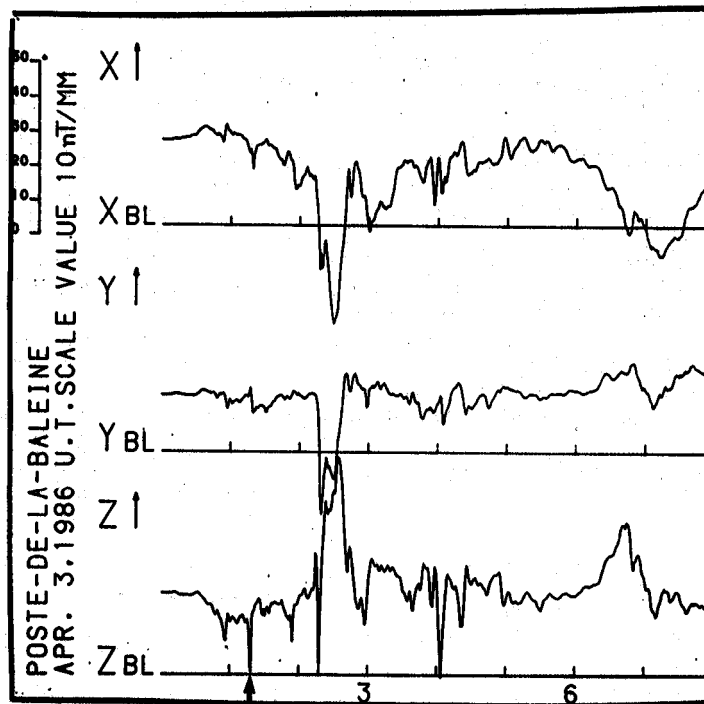 intensification (featuring the development of a localized current filament as discussed above) involves a characteristic Pi 2 wavelet as shown in Figure 17a, with a multiple onset substorm involving many such wavelets which, when strung together with appropriate phasing, provide the appearance of a pulsation wave train (Figure 17b). The amplitudes of Pi 2 wavelets can reach a few tens of nT in the near vicinity of filament formation, however amplitudes a fraction of an nT up to a few nT are more typical for stations more than ~ 100 km away from the source region. Pi 2 pulsations are often used to time the onset of a substorm expansive phase or its subsequent intensifications. In this respect, it is important that researchers do not set some arbitrary magnitude threshold at single stations on which they base the conclusion that an onset/intensification did or did not occur. The onset of a clear Pi 2 wavelet clearly defines the time of the explosive growth of a substorm expansive phase current filament. However, the absence of a clearly defined Pi2 wavelet may merely indicate that the source was well removed from the available observation point(s).

Finally, it is interesting to note that there may even be structure in the filamentary currents whose appearance marks expansive phase onsets or intensifications. However, the scale size of such structures is actually <100 km and, since ground magnetometers are located at distances in excess of 100 km from the source current systems, it is impossible for ground based magnetometer arrays to study the evolution of current structure within the expansive phase filaments.

INTERPRETATION OF LATITUDE AND LONGITUDE PROFILES OF GROUND BASED MAGNETOMETER DATA

Earlier in this paper, we have shown in Figure 8 the expected magnetic perturbation pattern for an east-west ionospheric electrojet. Under the assumption that the electrojet is of infinite length, the perturbations only appear in the H- and Z- components. The eastward and westward electrojets due to directly driven activity are both very long and can be treated as infinite sheet currents of limited latitudinal width for purposes of identifying electrojet width and strength in the local time sector of the observations. Figure 18 shows a latitude profile taken in the afternoon sector featuring a clear eastward electrojet. Using the quantitative modeling techniques developed by Kisabeth [1972], it can be shown that the electrojet lies between the positive and negative extrema in the Z-component profile. Those same modeling techniques can be used to evaluate the strength of the current flowing in the electrojet. What is noticeable in Figure 18 is the level shift in the D-component across the latitude span of the electrojet. Based on the results of Hughes and Rostoker [1977, 1979], this level shift is interpretable in terms of a sheet of upward field-aligned current flow spanning the poleward portion of the electrojet. While the D-component carries information about the net upward or downward field-aligned current integrated along the meridian of the observations, that same component can also give information about azimuthal asymmetries in the current flow along the auroral oval. This is particularly valuable for the study of auroral surges and omega bands which accompany magnetospheric substorm activity. For studies of localized current structures within the oval, it is useful to have profiles of the magnetic perturbations along lines of both constant magnetic latitude and longitude. To give some indication of how one goes about interpreting these longitude and latitude
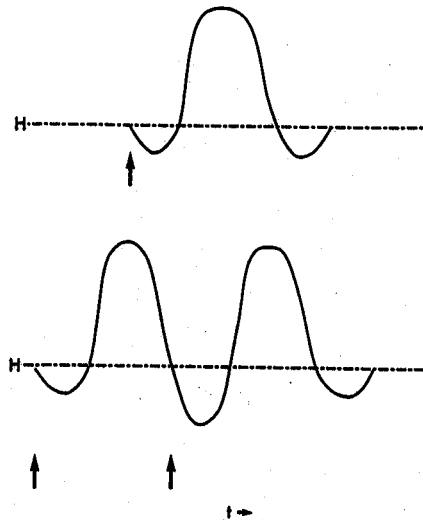
Figure 17.   Panel A shows the magnetic signature of a Pi 2
pulsation which accompanies the onset of a single filamentary
current system such as that shown in Figure 16.   Panel B shows
that the overall Pi 2 activity accompanying a multiple onset
substorm consists of a number of these wavelets strung
together.   If the phasing of the wavelets is appropriate, the
effect is that of a lengthy Pi 2 wavetrain as in the case of
the two wavelets whose onsets (vertical arrows) are shown in
Panel B.
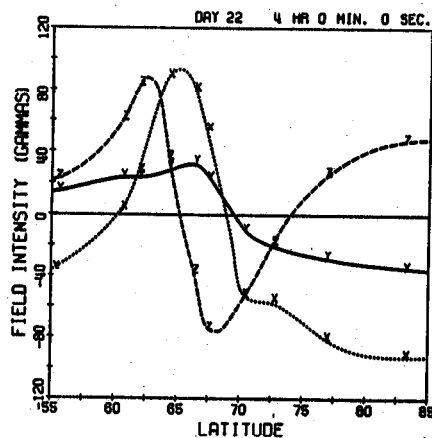
Figure 18.   Latitude profile taken by the University of
Alberta meridian line of magnetometers across the eastward
electrojet   in   the   early   evening   sector   (~2000   MLT)   on
January 22, 1972.   The electrojet current is distributed be-
tween the extrema in the Z-component profile while the nega-
tive level shift in the D-component from 67-70° is indicative
of the presence of net upward field-aligned current flow in an
east-west aligned current sheet crossing the meridian line of
magnetometers.

profiles, we show in Figures 19a and 19b profiles taken during the development of an auroral surge associated with a substorm expansive phase.

Figure 19a shows, in Panel A the latitude profile across the auroral oval just prior to the development of a surge in the vicinity of the magnetometer array. The signature is that of a weak westward electrojet crossing the meridian line between 65° and 68° N. Panels B1, B2 and C in the same figure show the distortion of the magnetic perturbation pattern as the surge develops. The latitudinally localized positive D-component regime in Panel B1 is the signature of the localized region of equatorward current flow along the western edge of the surge form. The marked distortions in the H- and Z-components along the meridian line make their interpretation difficult based on Figure 19a alone. Figure 19b shows the corresponding data for the east-west line of stations (the north-south and east-west lines together forming a cross). Just prior to the appearance of the surge, Panel A shows H- and D-component signatures of a westward electrojet that changes its strength but little over the approximately one time zone of coverage. The increasing positive Z from west to east indicates that the electrojet is aligned from south-east to north-west, with the station to the north west being relatively close to the center of the electrojet. Panels B1, B2 and C show the longitudinal localization of the positive D-component regime associated with the surge. The movement of the positive peak in ΔD along with its zero crossover point and the negative peak in ΔZ are the signatures of the western expansion of the western edge of the surge as it evolves. The reader is referred to Tighe and Rostoker [1981] and Kawasaki and Rostoker [1979] for more detailed descriptions of the use of latitude and longitude profiles to diagnose the development of structures of localized east-west extent in the auroral oval.

EFFECTS OF INDUCED CURRENTS IN THE EARTH

No commentary on the interpretation of ground based data would be complete without a warning to the reader that any changes in the source current systems above the earth will induce electric currents in the conducting earth below the observation point (on or above the earth's surface). Thus the magnetic field perturbations recorded by a ground based magnetometer reflect the sum of the contributions from the source currents and the induced earth currents. In principle, it is possible to construct integral expressions for the separation of the internal and external contributions to the total perturbation magnetic field (Porath et al., 1970). However, in reality there is insufficient data available to permit such a separation of fields so that treatment of a time dependent problem involving finite subsurface conductivities is not viable. However, there have been several solutions proposed to the time-independent problem where the Earth is considered to be an insulator from the surface to some specified depth and a perfect conductor below that depth (cf. Bonnevier et al., 1970; Ashour, 1971; Kisabeth and Rostoker, 1977). For the purposes of studying three dimensional current systems of the type flowing during substorm activity, the approaches of Bonnevier et al. and Kisabeth and Rostoker are the most effective. In the former case, the authors considered each three dimensional current loop to be the sum of infinitesimal current loops around each surface element such that, if they are added together, the current cancels everywhere except at the border of the surface (see Figure 20). In this fashion, the magnetic perturbation from the three dimensional current loop can be considered as the sum of the contributions from a distribution of magnetic dipoles whose moments

-A-

DAY: 307 06:35:35.0 (UT)

-B1-

DAY: 307 06:43:15.8 (UT)

-B2-

DAY: 307 06:44:17.3 (UT)

-C-

DAY: 307 06:48:30.7 (UT)
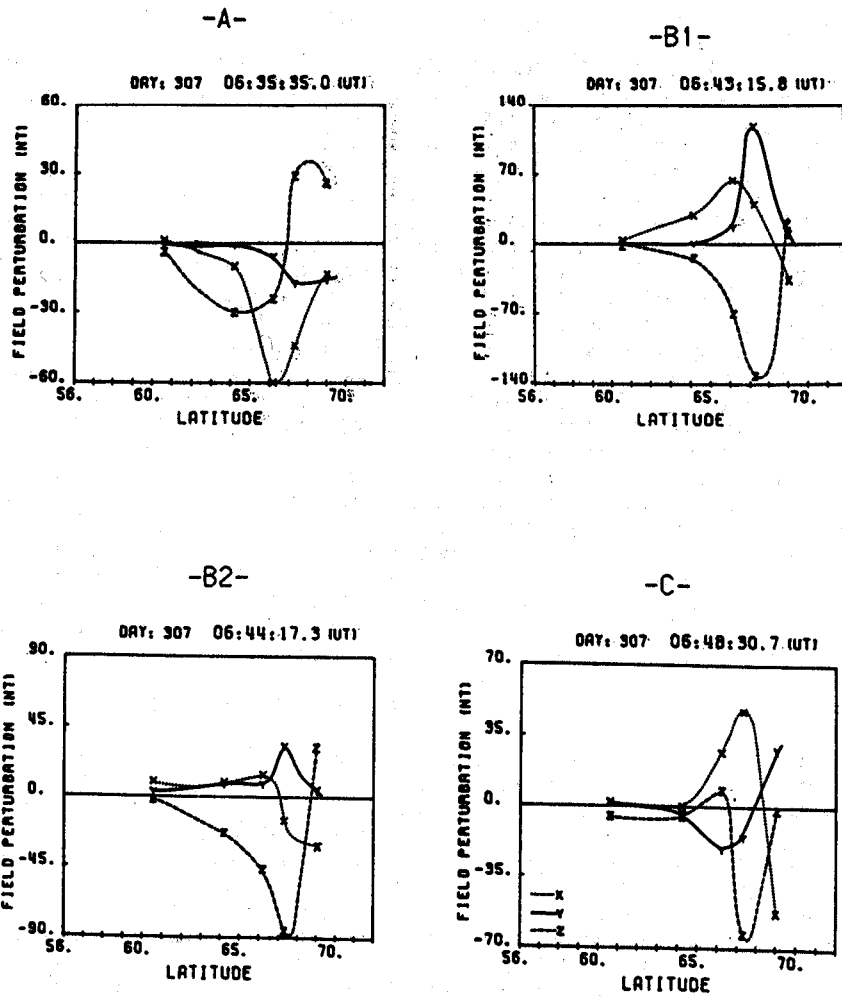
Figure 19a. Latitude profiles from a cross array showing the
electrojet configuration just prior to the development of a
surge near the meridian line (Panel A) and at three instants
after the surge begins to develop (Panels B1, B2 and C) (Tighe
and Rostoker, 1981).

-A-

DAY: 307   06:35:35.0 (UT)

-B1-

DAY: 307   06:43:15.8 (UT)

-B2-

DAY: 307   06:44:17.3 (UT)

-C-

DAY: 307   06:48:30.7 (UT)

Figure 19b. Longitude profiles from the cross array alluded to in Figure 19a for equivalent moments during the substorm evolution described by the latitude profiles shown in that Figure (Tighe and Rostoker, 1981).

Figure 20. Geometry of the dipole current elements used to compute the magnetic effects of the three dimensional current loops descriptive of the substorm current wedge (Bonnevier et al., 1970).

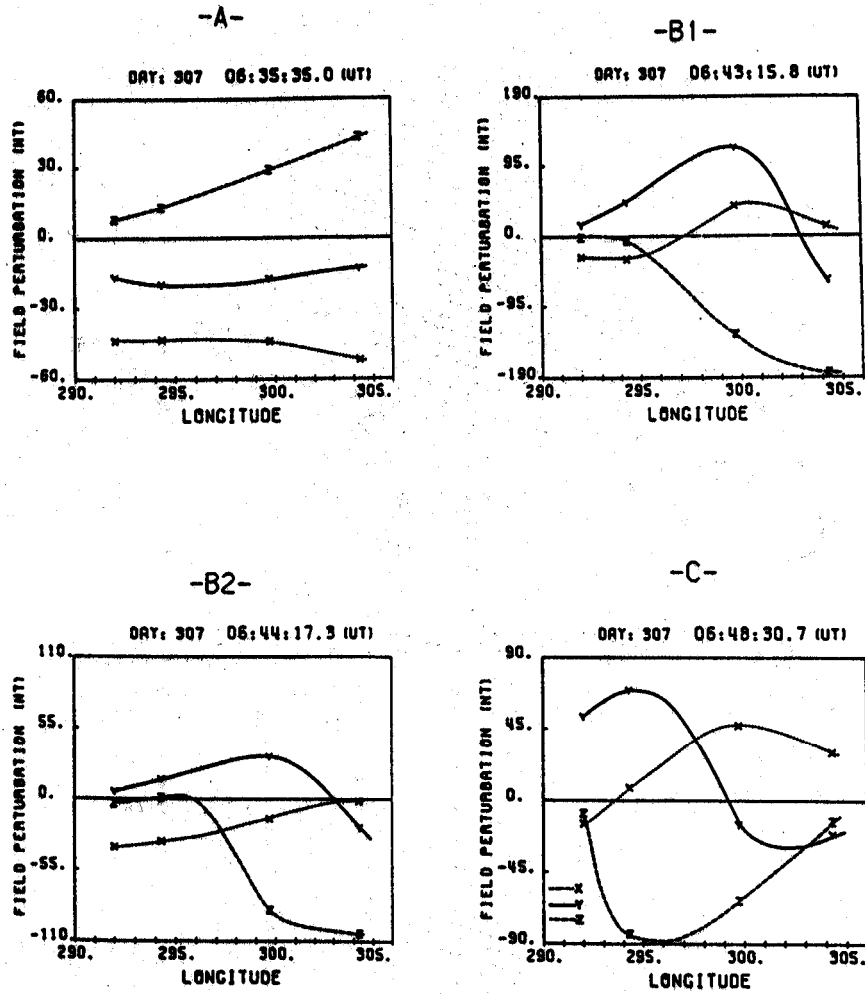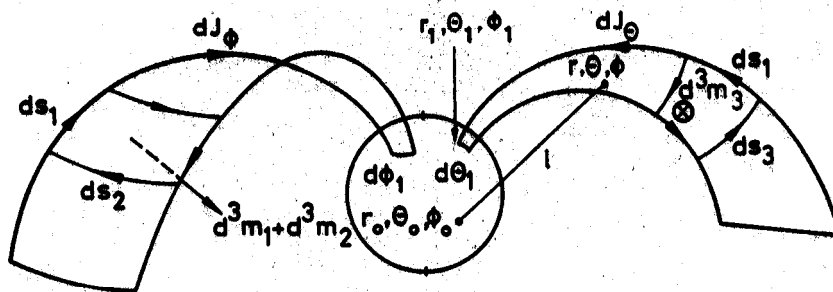$$\underline{d^3m} = d^3m_1 \; \hat{\underline{r}} + d^3m_2\hat{\underline{\Theta}} + d^3m_3\hat{\underline{\phi}} \qquad\qquad [4]$$

are given by the size and orientation of the surface elements and the current in the loops. If one then considers the Earth to be represented by a perfect conductor from the center to radius r_2 and an insulator from r_2 to the surface, then the magnetic effect of the induced currents can be represented by image dipoles located within the conductor. For the radial component of the external dipole contribution (cf. Eq. 4), one obtains an image dipole with a moment $(- r_2{}^3/r^3)$ $\underline{d^3m_1}$ located at the inverse point of the external dipole (i.e. at a distance $r^1 = r_2{}^2/r$ from the center). For $\underline{d^3m_2}$ and $\underline{d^3m_3}$, one gets similar image dipoles parallel to the external ones at the inverse point plus a dipole distribution along a straight line between the center $x = 0$ and the inverse point $x = r^1$ with the moments $- (x \, dx/r \; r_2) \, [\underline{d^3m_2} + \underline{d^3m_3}]$. The total disturbance field is then obtained by adding the contributions of the external and image dipoles at each field point where the perturbation field is desired. As an example of the influence of induced currents in the Earth, we show in Table 1 the ratio of internal to external field contributions at various latitudes for a three dimensional current loop involving a westward electrojet of length $20°$ located with its center at $67.5°N$ and having a width of $5°$ of latitude. The ratios shown in Table 1 are calculated for depths of the perfect conductor ranging from 100 km to 300 km. This is because, in line with the expectation for skin depths of the real Earth, we should expect the perfect conductor to be close to the surface for high frequency disturbances and deeper for low frequency disturbances. For disturbances having the time scale of substorms, Kisabeth [1972] has found that 250 km is the most appropriate depth for the surface of the perfect conductor. The effect of subsurface conductivity is to increase the magnitude of the horizontal component of the magnetic perturbation while decreasing the vertical component. For a flat earth approximation and an infinite line current source, the correction factors are 2/3 and 2 for the horizontal and vertical components respectively. The ratios shown in Table 1 clearly show that such a uniform treatment for all field points is not justified, and it is necessary to know the distance of the observation point from the source current distribution as well as the geometry of the source current distribution if one is to effectively correct for Earth induction effects.

Finally, it is important to note that the treatment of the induction problem shown above is only appropriate if there are no regions of anomalous subsurface conductivity in the vicinity of the observation points. Unfortunately, the Earth is far from having a uniform conductivity and sharp discontinuities are often found near tectonically active regions in addition to regions that have been tectonically active in the distant past. As well, the effects of seawater together with the upwelling of the Earth's mantle at continental margins make rather suspect the interpretation of magnetic perturbations from substorms detected by stations near coastlines. The reader is referred to Rikitake [1966] for a more detailed description of the effects of subsurface conductivity anomalies on the perturbation magnetic field detected at the Earth's surface together with the analytical techniques one can use to establish the presence of such anomalies.

INFERENCE OF MAGNETOSPHERIC AND IONOSPHERIC ELECTROMAGNETIC PROPERTIES FROM QUANTITATIVE MODELING USING GROUND BASED MAGNETOMETER ARRAY DATA

Up till now, this paper has concentrated on providing a qualitative description of how one goes about interpreting the signatures found in ground magnetometer data. However, one should hope that such information can provide a more quantitative assessment of the spatial extent of the disturbed regions

Table 1: Ratio of the total perturbation magnetic field due to internal induced currents to the total perturbation magnetic field due to external inducing currents from a three dimensional current system (Figure 9) for different observation points on the surface of the perfect conductor below the Earth's surface.

Latitude	100 km	200 km	300 km
55°	0.836	0.691	0.560
60°	0.736	0.526	0.375
65°	0.416	0.221	0.133
67.5°	0.452	0.238	0.142
70°	0.400	0.210	0.127
75°	0.751	0.532	0.377
80°	0.874	0.725	0.590
84.5°	0.924	0.816	0.709

of the ionosphere and the possibility of estimating some of the more crucial parameters through which one might hope to quantify the level of the solar terrestrial interaction. During the early part of the 1970's, analytical routines were developed which permitted the magnetic perturbation from three dimensional current systems to be evaluated at any point on the Earth's surface (cf. Bonnevier et al., 1970; Kisabeth and Rostoker, 1977; Kisabeth, 1979). While these calculations were relevant to current flow in a dipolar magnetic field geometry, the fact that most of the perturbation detected on the surface of the Earth comes from current flow relatively close to the Earth made such model calculations rather useful. However, in order to achieve further progress, it is necessary to have the current flow set in a more realistic geometry involving high latitude currents flowing out into the deep magnetotail instead of being confined to dipole geometry. For this reason, we will not develop the codes used to compute perturbations from three dimensional current systems in a dipole magnetic field in this paper. The reader can find the details in the papers quoted above along with full comparisons of the various approaches to the problem in Kisabeth [1972].

By the beginning of the 1980's, a new approach to modeling was coming to the fore. This method emphasized the physics of ionospheric current flow and the reasons for the divergence of this flow along magnetic field lines so as to produce the three dimensional current loops which couple the ionosphere and magnetosphere. Development of the codes to implement this modeling scheme proceeded independently in the U.S.S.R. (cf. Bazarzhapov et al., 1979; Mishin et al., 1980) and in the U.S.A. (cf. Kamide and Matsushita, 1979a, 1979b; Kamide et al., 1981) leading to the ability to infer information about the distribution of ionospheric currents, field-aligned currents and electric fields in the high latitude regions of the Earth. In the light of the importance of the development of such algorithms for the effective utilization of ground based magnetometer observations, we shall briefly outline the basis of this modeling approach as developed by Kamide et al. [1981] (known as the KRM technique).

One begins by utilizing the world wide network of magnetometers to establish the equivalent current system at some point in time. Here the horizontal magnetic perturbation vectors are computed (subtracting the quiet time values from the measured values and making some effort to correct for Earth induction effects) and the equivalent current system constructed by drawing smooth curves of equivalent current flow. If one describes the equivalent current flow lines by the scalar potential function Ψ, the equivalent current density (in A/m) can be expressed in the form

$$\underline{i}_T = \underline{n}_r \times \text{grad } \Psi \qquad [5]$$

where $\underline{n}_r$ is a unit radial vector. Outside of the region of real current flow, the measured magnetic perturbation can be expressed as the gradient of a magnetic scalar potential, viz.

$$\underline{b} = - \text{grad } V \qquad [6]$$

and Chapman and Bartels [1940] (pg. 631) have shown that the external portion of V is related to Ψ by straightforward mathematical expressions.

The KRM technique proceeds on the basis that, once one knows the equivalent current function Ψ, one can assume a reasonable conductivity distribution (for which one must have an analytical expression) and derive the ionospheric electric field, the real horizontal current and the field-aligned current under the following set of assumptions:

(1) The electric field is purely electrostatic.

(2) Geomagnetic field lines are electric equipotentials.

(3) The dynamo effect of neutral winds can be ignored.

(4) Magnetic contributions due to magnetospheric ring currents, tail currents and magnetopause currents can be ignored.

(5) Geomagnetic field lines are effectively radial, implying that errors due to the fact that field-aligned currents actually follow the quasi-dipolar magnetic field lines can be ignored.

The next step involves the expression of the total height-integrated horizontal ionospheric current as the sum of the equivalent current and a "potential" current $\underline{i}_P$, viz.

$$\underline{i} = \underline{i}_T + \underline{i}_P \qquad [7]$$

where $\underline{i}_P$ can be expressed in terms of a current potential τ, viz.

$$\underline{i}_P = - \text{grad } \tau \qquad [8]$$

such that div $\underline{i}_T = 0$ and curl $\underline{i}_P = 0$ and the field aligned-current density is given by

$$j_{||} = \text{div } \underline{i} = \text{div } \underline{i}_P \qquad [9]$$

where $j_{||}$ is positive downwards.

The real horizontal ionospheric current is related to the electric field $\underline{E}$ (in a frame of reference corotating with the Earth) through the expression

$$\underline{i} = \Sigma_P \underline{E} + \Sigma_H \underline{E} \times \underline{n}_r \qquad [10]$$

where

$$\Sigma_P = \int_o^h \sigma_P \, dr$$

and

$$\Sigma_H = \int_o^h \sigma_H \, dr$$

are the height-integrated Pedersen and Hall conductivities respectively, with σ_P and σ_H being the respective specific conductivities. Finally, one expresses the electric field in terms of scalar potential

$$\underline{E} = - \text{grad } \Phi \qquad [11]$$

and obtains a partial differential equation for Φ in terms of Ψ by equating the right hand sides of Eq (7) and Eq (10) and taking the curl of the resulting expression. In spherical coordinates, where θ is the colatitude and λ is the east longitude, one obtains

$$A \frac{\partial^2 \Phi}{\partial \theta^2} + B \frac{\partial \Phi}{\partial \theta} + C \frac{\partial^2 \Phi}{\partial \lambda^2} + D \frac{\partial \Phi}{\partial \lambda} = F \qquad [12]$$

where the coefficients in the above equation are given by

$$A = (\sin \theta) \Sigma_H$$

$$B = \frac{\partial}{\partial \theta} ((\sin \theta) \Sigma_H) + \frac{\partial}{\partial \lambda} \Sigma_P$$

$$C = \Sigma_H / \sin \theta$$

$$D = \frac{\partial}{\partial \theta} \Sigma_P - \frac{\partial}{\partial \lambda} (\Sigma_H / \sin \theta)$$

$$F = \frac{\partial}{\partial \theta} (\sin \theta \frac{\partial \Psi}{\partial \theta}) + (1/\sin \theta) \frac{\partial^2 \Psi}{\partial \lambda^2}$$

Eq (12) is solved using the boundary conditions

$$\Phi (0, \lambda) = 0 \qquad (13)$$

$$\frac{\partial \Phi}{\partial \theta} (\pi/2, \lambda) = 0 \qquad (14)$$

where the equatorial boundary condition expressed in Eq (14) is in place only for numerical convenience and has no physical basis in fact. A finite difference scheme is then used to solve the partial differential Eq (12) yielding the form of the electrostatic potential Φ. The ionospheric electric field can then be obtained from

$$E_\theta = - \frac{\partial \Phi}{a \partial \theta} \qquad E_\lambda = - \frac{\partial \Phi}{a \sin \theta \partial \lambda} \qquad (15)$$

where a is the distance from the center of the earth to the (thin) ionosphere. Using the values of E_θ and E_λ and reformulating the height-integrated conductivities in the (λ, θ) coordinate system, viz.

$$\underline{\underline{\Sigma}} = \begin{bmatrix} \Sigma_P & \Sigma_H \\ -\Sigma_H & \Sigma_P \end{bmatrix} = \begin{bmatrix} \Sigma_{\theta\theta} & \Sigma_{\theta\lambda} \\ -\Sigma_{\lambda\theta} & \Sigma_{\lambda\lambda} \end{bmatrix}$$

the ionospheric current can be expressed in the form

$$\begin{bmatrix} j_\theta \\ j_\lambda \end{bmatrix} = \begin{bmatrix} \Sigma_{\theta\theta} & \Sigma_{\theta\lambda} \\ -\Sigma_{\theta\lambda} & \Sigma_{\lambda\lambda} \end{bmatrix} \begin{bmatrix} E_\theta \\ E_\lambda \end{bmatrix} \qquad (16)$$

Finally, by inserting the information about the real ionospheric current from Eq (16) into Eq (9), one can obtain the field-aligned current. Kamide et al. used the accelerated Liebmann over-relaxation method (Gary, 1969) involving an iteration technique to minimize a convergence parameter in order to evaluate the current and electric field values over the grid of field points.

To demonstrate the capability of the KRM algorithm, we show in Figure 21 the output for a run performed for ground data obtained over the interval May-June 1965 during disturbed days. The height-integrated conductivities due to energetic particle precipitation were approximated by the expressions

$$\Sigma_P = \Sigma_m \exp\left[-\frac{(\theta-\theta_o)^2}{D_\theta^2} - \frac{(\lambda - \lambda_o)^2}{D_\lambda^2}\right]$$

$$\Sigma_H = k\Sigma_P \tag{17}$$

and these values were superposed on an appropriate conductivity distribution due to the incidence of solar radiation on the ionosphere. In Eq (17), (θ_o,λ_o) gives the position of the center of the region of enhanced conductivity while D_θ and D_λ specify the Gaussian distribution for the latitudinal and longitudinal directions respectively with Σ_m and k being constants. Figure 21a shows the equivalent current system for the interval in question as a polar projection in geomagnetic coordinates; this information constituted the input to the routine obtained using ground based magnetometer data. Figure 21b shows the equipotential distribution in the same polar plot format, this figure containing the calculated information for the ionospheric electric field. Figure 21c shows the real ionospheric current vectors for latitudes higher than 50° in which the eastward and westward directly driven electrojets are clearly evident. Finally, Figure 21d gives the field-aligned current distribution, in which the anti parallel pairs of current sheets discovered by Zmuda and Armstrong [1974] are apparent.

Ultimately, if one were to have an ideal two dimensional grid of magnetometer station covering the Earth's surface (grid spacing 1° x 1°) it would be possible to obtain a very accurate picture of the key electric field and current parameters, limited only by the inaccuracies of the conductivity distribution. However, in reality the available magnetometer stations are quite limited in number and irregularly spaced over the Earth's surface. Using only information about the horizontal components of the perturbation magnetic field, it is quite possible to be significantly in error in one's estimate of the current and field parameters. For example, if one were to have only one station in a given longitudinal sector and the station were to fortuitously lie at the interface between the eastward and westward electrojets in the evening sector, a zero horizontal perturbation magnetic field could be measured leading to the incorrect conclusion that no electrojet currents crossed the meridian of the station. Such a false conclusion would be used by the algorithm to produce entirely meaningless results regarding the currents and electric field anywhere in the vicinity of the unfortunately placed station. It is possible to partly alleviate this problem by using information from the Z-components of the magnetic perturbations at the many stations in the array. Combined with a reasonable forward model of the electrojet structure across the meridian of each observatory, it is possible to use information about the Z/H ratio to infer

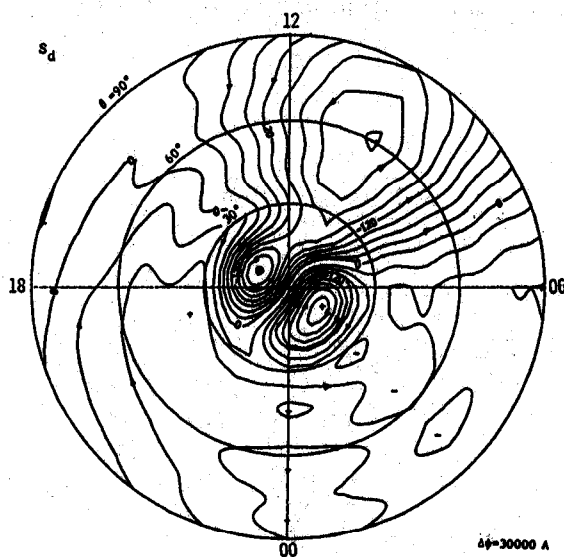## EQUIVALENT IONOSPHERIC CURRENT SYSTEM

Figure 21a. Equivalent current system for disturbed days cal-
culated by averaging data over the interval May - June 1965.
This set of data obtained from ground magnetometer recordings
constitutes the input for the KRM modeling routine (Kamide et
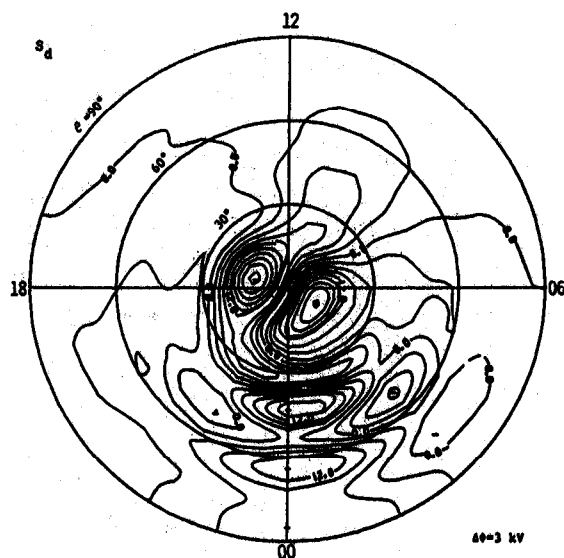al., 1981).

ELECTRIC POTENTIAL

Figure 21b. Equipotential distribution calculated using the
KRM algorithm for the data portrayed in Figure 21a (Kamide et
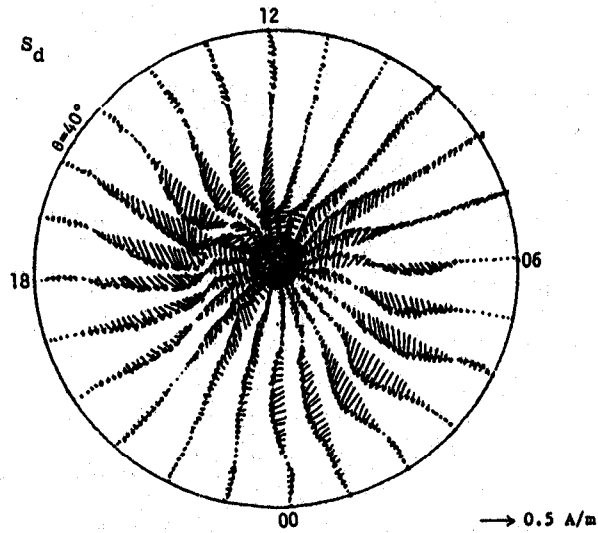al., 1981).

IONOSPHERIC CURRENT VECTORS

Figure 21c. Real ionospheric current vectors calculated using the KRM algorithm for the data portrayed in Figure 21a (Kamide et al., 1981).
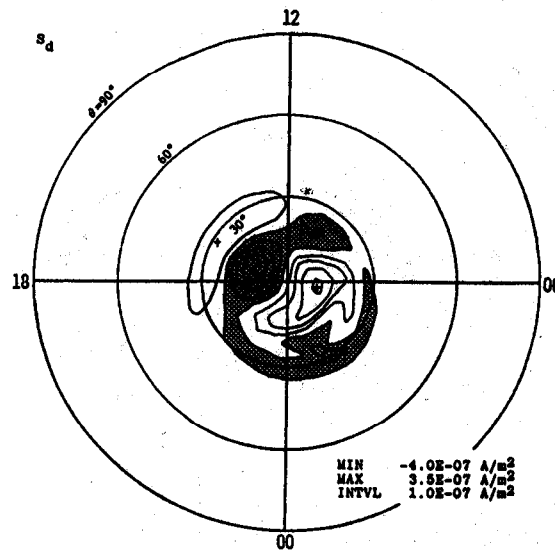
FIELD-ALIGNED CURRENTS

Figure 21d.   Field-aligned current distribution calculated using the KRM algorithm for the data portrayed in Figure 21a (Kamide et al., 1981). The shaded region indicates upward current flow.

information about the maximum H-component perturbation along the meridian
passing through the observatory. In some cases, it might be possible to use
linear inversion techniques (Hughes et al., 1979) coupled with an appropriate
forward model of the electrojet structure to accurately quantify the strength
of the ionospheric current flow across a meridian along which observatories
were arrayed with reasonable latitudinal separation.

Ultimately, it may be possible to use luminosity distributions obtained
from imagers aboard high altitude satellites to infer useful information about
the conductivity distribution in the high latitude ionosphere (cf. Marklund et
al., 1987). Since such luminosity information might also yield the position of
the poleward and equatorward borders of the auroral current systems, it may yet
be possible to put additional constraints on the KRM technique in such a manner
as to produce yet more reliable information on the instantaneous current and
electric field configuration in the high latitude ionosphere.

CONCLUDING REMARKS

In this paper, I have tried to demonstrate how ground based magnetometer
data can be used to infer information about the three-dimensional electric
current systems which couple the magnetosphere to the ionosphere. It must be
emphasized that magnetometer data from stations confined to the Earth's surface
cannot, by themselves, provide a non-unique representation of the electric
current systems external to the Earth. However, combined with information
obtained from polar orbiting satellites carrying particle and field detectors,
it has been possible to construct reasonable forward models for the current
systems. The interpretation of ground magnetometer data presented in this
paper has drawn on the wealth of correlations described in the literature
between ground magnetometer data and polar orbiting satellite data to give a
useful tool to the student of the solar-terrestrial interaction. While there
is still considerable research to be done in identifying the signatures of
relatively small scale current systems involved with auroral forms, the reader
should feel comfortable in using the techniques described in this paper for the
study of directly driven magnetospheric activity as well as many aspects of
substorm expansive phase behaviour.

ACKNOWLEDGEMENTS

REFERENCES

Ashour, A. A., The evaluation of the field of the currents induced in the Earth by an external field whose distribution is known numerically, Radio Sci., 6, 171, 1971.

Axford, W. I. and C. O Hines, A unifying theory of high-latitude geophysical phenomena and geomagnetic storms, Can. J. Phys., 39, 1443, 1961.

Bannister, J. R. and D. I. Gough, Development of a polar magnetic substorm: a two dimensional magnetometer array study, Geophys. J. R. Astr. Soc., 51, 75, 1977.

Bonnevier, B., R. Boström; and G. Rostoker, A three dimensional model current system for polar magnetic substorms, J. Geophys. Res., 75, 107, 1970.

Baumjohann, W., Ionospheric and field-aligned current systems in the auroral zone: a concise review, in Advances in Space Research., 2, 55, 1983.

Bazarzhapov, A. D., V. M. Mishin, D. S. Shirapov and G. B. Shpynev, Electric fields and currents in the quiet magnetosphere as determined from ground measurements, Issle. Geomag. Aeron. Fiz. Solntsa, 46, 13, 1979.

Chapman, S. and J. Bartels, Geomagnetism, Oxford Univ. Press (Clarendon), London, 1940.

Dungey, J. W., Interplanetary magnetic field and the auroral zones, Phys. Rev. Lett., 6, 47, 1961.

Eastman, T. E., L. A. Frank and C. Y. Huang, The boundary layers as the primary transport regions of the earth's magnetotail. J. Geophys. Res., 90, 9541, 1985.

Fukushima, N., Polar magnetic storms and geomagnetic bays, J. Fac. Sci. Tokyo Univ. 8, 293, 1953.

Gary, J., The numerical solution of partial differential equations, NCAR MS 69 - 54, Nat. Cent. for Atmosph. Res., Boulder, CO, 1969.

Goertz, C. K. and R. A. Smith, The thermal catastrophe model of substorms, J. Geophys. Res., 94, 6581, 1989.

Hakura, Y., Tables and maps of geomagnetic coordinates corrected by the higher order spherical harmonic terms, Rept. Ionos. Space Res., Japan 19, 121, 1965.

Harang, L., The mean field of disturbance of polar geomagnetic storms, Terrest. Mag. Atmos. Elec. 51, 353, 1946.

Heppner, J. P., J. D. Stolarik and E. M. Wescott, Electric field measurements and the identification of currents causing magnetic disturbances in the polar cap, J. Geophys. Res., 76, 6028, 1971.

Hines, C. O., The energization of plasma in the magnetosphere: hydromagnetic and particle-drift approaches, Planet. Space Sci., 10, 239, 1963.

Hughes, T. J., and G. Rostoker, Current flow in the magnetosphere and ionosphere during periods of moderate activity, J. Geophys. Res., 82, 2271, 1977.

Hughes, T. J. and G. Rostoker, A comprehensive model current system for high latitude magnetic activity - I. The steady state systems, Geophys. J. Roy. astron. Soc., 58, 525, 1979.

Hughes, T. J., D. W. Oldenburg and G. Rostoker, Interpretation of auroral oval equivalent current flow near dusk using inversion techniques, J. Geophys. Res., 84, 450, 1979.

Kamide, Y. and S. Matsushita, Simulation studies of ionospheric electric fields and currents in relation to field-aligned currents, 1. Quiet periods, J. Geophys. Res., 84, 4083, 1979a.

Kamide, Y. and S. Matsushita, Simulation studies of ionospheric electric fields and currents in relation to field-aligned currents, 2. Substorms, J. Geophys. Res., 84, 4099, 1979b.

Kamide, Y., A. D. Richmond and S. Matsushita, Estimation of ionospheric electric field, ionospheric currents, and field aligned currents from ground magnetic records, J. Geophys. Res., 86, 801, 1981.

Kamide, Y., B.-H. Ahn, S. -I Akasofu, W. Baumjohann, E. Friis-Christensen, H. W. Kroehl, H. Maurer, A. D. Richmond, G. Rostoker, R. W. Spiro, J. K. Walker and A. N. Zaitzev, Global distribution of ionospheric and field-aligned currents during substorms determined with magnetic data from six IMS meridan chains: initial results, J. Geophys. Res., 87, 8228, 1982.

Kawasaki, K. and G. Rostoker, Perturbations magnetic fields and current systems associated with eastward drifting auroral structures, J. Geophys. Res., 84, 1464, 1979.

Kisabeth, J. L., The dynamical development of the polar electrojets., Ph.D. Thesis, University of Alberta, Edmonton, Alberta, Canada 1972.

Kisabeth, J. L., On calculating magnetic and vector potential fields due to large-scale magnetospheric current systems and induced currents in an infinitely conducting earth, in: Quantitative Modeling of Magnetospheric Processes, ed. by W. P. Olson, American Geophysical Union, Washington, D. C., p. 473, 1979.

Kisabeth, J. L. and G. Rostoker, The expansive phase of magnetospheric substorms, 1. Development of the auroral electrojets and auroral arc configuration during a substorm, J. Geophys. Res., 79, 972, 1974.

Kisabeth, J. L. and G. Rostoker, Modelling of three-dimensional current systems associated with magnetospheric substorms, Geophys. J. Roy. Astron. Soc., 49, 655, 1977.

Lundin, R., On the magnetospheric boundary layer and solar wind energy transfer into the magnetosphere, Space. Sci. Rev., 48, 263, 1988.

Marklund, G. T., L. G. Blomberg, T. A. Potemra, J. S. Murphree, F. J. Rich and K. Stasiewicz, A new method to derive "instantaneous" high latitude potential distributions from satellite measurements including auroral imager data, Geophys. Res. Lett., 14, 439, 1987.

Mishin, V. M., A. D. Bazarzhapov and G. B. Shpynev, Electric fields and currents in the earth's magnetosphere, in Dynamics of the Magnetosphere, ed. by S. -I. Akasofu, p. 249, D. Reidel Publ. Co., Hingham, MA, 1980.

Perreault, P. and S. -I. Akasofu, A study of geomagnetic storms, Geophys. J. Roy. astron. Soc., 54, 547, 1978.

Porath, H., D. W. Oldenburg, and D. I. Gough, Separation of magnetic variation fields and conductive structures in the Western United States, Geophys. J. Roy. astr. Soc. 19, 237, 1970.

Pytte, T., R. L. McPherron and S. Kokubun, The ground signatures of the expansion phase during multiple onset substorms, Planet. Space Sci., 24, 1115, 1976.

Rikitake, T., Electromagnetism and the Earth's Interior, Elsevier Publ. Co., New York, 1966.

Rostoker, G., Midlatitude transition bays and their relation to the spatial movement of overhead current systems, J. Geophys. Res., 71, 79, 1966.

Rostoker, G., Macrostructure of geomagnetic bays, J. Geophys. Res., 73, 4217, 1968.

Rostoker, G., Geomagnetic indices, Rev. Geophys. Space Phys., 10, 935, 1972.

Rostoker, G., Interpretation of magnetic field variations during substorms, in Earth's Magnetospheric Processes, ed. by B. M. McCormac, p. 379, D. Reidel Publ. Co., 1972.

Rostoker, G., Overview of observations and models of auroral substorms, in Auroral Physics, ed. by C.-I. Meng, Cambridge Univ. Press, 1989, (in press).

Rostoker, G., C. W. Anderson III. D. W. Oldenburg, P. A. Camfield, D. I. Gough, and H. Porath, Development of a polar magnetic substorm current system, J. Geophys. Res., 75, 6318, 1970.

Rostoker, G. and R. Boström, A mechanism for driving the gross Birkeland current configuration in the auroral oval, J. Geophys. Res., 81, 235, 1976.

Rostoker, G. and M. Mareschal, Field-aligned current and the auroral electrojets in the post-noon quadrant, J. Geophys. Res., 87, 9071, 1982.

Rostoker, G., S. -I. Akasofu, J. Foster, R. A. Greenwald, Y. Kamide, K. Kawasaki, A.T.Y. Lui, R. L. McPherron and C. T. Russell, Magnetospheric substorms - definition and signatures, J. Geophys. Res., 85, 1663, 1980.

Saito, T., Oscillation of geomagnetic field with the progress of pt-type pulsation, Sci. Rept. Tohoku Univ., 5, Geophys. 13, 53, 1961.

Silsbee, H. C. and E. H. Vestine, Geomagnetic bays, their occurrence frequency and current systems, Terr. Magn. Atmos. Elec., 47, 195, 1942.

Tighe, W. G. and G. Rostoker, Characteristics of westward travelling surges during magnetospheric substorms, J. Geophys., 50, 51, 1981.

Wiens, R. G. and G. Rostoker, Characteristics of the development of the westward electrojet during the expansive phase of magnetospheric substorms, J. Geophys. Res., 80, 2109, 1975.

Zmuda, A. J. and J. C. Armstrong, The diurnal flow of field-aligned currents, J. Geophys. Res., 79, 4611, 1974.